URS

VIBRATION TESTING OF AN EPOXY-REPAIRED REINFORCED CONCRETE TEST STRUCTURE

G. Norman Owen
Ike O. Egbuonye
Onder Kustu
Roger E. Scholl

prepared for
the National Science Foundation
Under Agreement CEE-7812714
and for the United States Department of Energy
Under Contract DE-AC08-81NV10145

prepared by
URS/John A. Blume & Associates, Engineers
130 Jessie Street (at New Montgomery)
San Francisco, California 94105

50272-101

REPORT DOCUMENTATION PAGE	1. REPORT NO. NSF/CEE-83210	2.	3. Recipient's Accession No. PB84 133925
4. Title and Subtitle: Vibration Testing of An Epoxy-Repaired Reinforced Concrete Test Structure			5. Report Date: March 1983 6.
7. Author(s): G.N. Owen, I.O. Egbuonye, O. Kustu, R.E. Scholl			8. Performing Organization Rept. No. JAB-10145-3
9. Performing Organization Name and Address: URS/John A. Blume & Associates, Engineers 130 Jessie Street (at New Montgomery) San Francisco, CA 94105			10. Project/Task/Work Unit No. 11. Contract(C) or Grant(G) No. (C) (G) CEE7812714
12. Sponsoring Organization Name and Address: Directorate for Engineering (ENG) National Science Foundation 1800 G Street, N.W. Washington, DC 20550			13. Type of Report & Period Covered 14.

15. Supplementary Notes

16. Abstract (Limit: 200 words)

Results are presented of a study of a full-scale, four-story reinforced concrete structure that was damaged by forced vibration and repaired by the epoxy-injection method. The structure was retested with low-amplitude vibrations, followed by forced vibrations. The damage to the epoxy-repaired structure was similar to that sustained by the original structure but the damage was less severe and the cracking was more widely distributed. Findings reveal that, for low-amplitude motions, the epoxy-repaired structure was slightly less stiff than the original undamaged structure. As the amplitude of the structure's response increased, the difference between the epoxy-repaired structure and the original structure decreased. At large deflections associated with severe damage, the epoxy-repaired structure was stiffer than the original structure.

17. Document Analysis a. Descriptors

Structures
Buildings
Reinforced concrete
Dynamic structural analysis
Cracking (fracturing)
Earthquake resistant structures
Vibration
Vibration tests
Stiffness
Stiffness tests
Epoxy compounds
Earthquakes

b. Identifiers/Open-Ended Terms

Epoxy injection method

R.E. Scholl, /PI

c. COSATI Field/Group

18. Availability Statement: NTIS	19. Security Class (This Report)	21. No. of Pages
	20. Security Class (This Page)	22. Price

(See ANSI-Z39.18) See Instructions on Reverse OPTIONAL FORM 272 (4-77) (Formerly NTIS-35) Department of Commerce

CONTENTS

CONTENTS (Continued)

page

TABLES

FIGURES

CONTENTS (Continued)

ACKNOWLEDGMENTS

The authors appreciate the financial support provided by the National Science Foundation for the vibration testing of an epoxy-repaired reinforced concrete test structure.

The Nevada Operations Office of the U.S. Department of Energy provided the test structure and the seismograph system, as well as overall administrative support for the project. It also provided the funding for the original destructive testing of the structure. The authors are particularly grateful for this continued interest and support from the Department of Energy.

Sandia National Laboratories provided the vibration generator and the technical support for the operation of the generator. Reynolds Electrical & Engineering Company, Inc., provided field support during the tests, and Pan American World Airways, DNA Photo Project, provided the photographic coverage.

The authors appreciate the assistance of the following individuals who provided support during the test operations, served as technical consultants, and/or reviewed this report: John A. Blume, John P. Banister, B. R. Bradley, D. M. Ellett, Kenneth K. Honda, Richard O. Navarro, Roger E. Skjei, and David O. Smallwood.

ABSTRACT

A full-scale, 4-story reinforced concrete structure, deliberately damaged by forced vibration in 1974, was repaired by the epoxy-injection method and retested in 1979 using the same reciprocating-mass vibration generator. The program consisted of a series of tests, beginning with low-amplitude vibrations, followed by forced vibrations, increased into the range of inelastic response of the structure. The test program was similar to the 1974 testing of the original, undamaged structure. Structural damage from the first destructive test was extensive, consisting of x-cracking and spalling at the beam-column connections. The 1979 damage to the epoxy-repaired structure was similar to that sustained by the original structure in 1974, but the cracking was more widely distributed, and, in general, damage was less severe following the 1979 test.

The results of this study show that, for low-amplitude motions, the epoxy-repaired structure was slightly less stiff than the original undamaged structure. However, a plot of the destructive-test data shows that, as the amplitude of the structure's response increased, the difference in stiffness between the epoxy-repaired structure and the original structure decreased. At large deflections associated with severe damage, the epoxy-repaired structure was actually stiffer than the original structure. The cracking at beam-column connections appeared to be much less severe in the 1979 test than in the 1974 test.

The behavior of the test structure, in both its original and epoxy-repaired states, was compared with that of theoretical models. The stiffness of models using moments of inertia for cracked sections, as recommended in the ACI 318-77 Commentary, are representative of the stiffness of the test structure as it begins to yield and to sustain visible damage.

1. INTRODUCTION

The philosophy of seismic design of buildings is that they should be engineered to resist major destructive earthquakes without collapse, although structural and nonstructural components in the buildings may sustain damage. While catastrophic collapses are theoretically avoided, structural damage is not. Following a major earthquake, each damaged building must be surveyed to determine whether it can be economically repaired and restored to service. One method commonly used to repair reinforced concrete structures is the injection of a high-strength epoxy compound into the cracked concrete, filling the voids and rebonding the fractured members.

Epoxy-injection techniques were used extensively to repair cracking of highway bridges, buildings, and other reinforced concrete structures damaged in a number of recent earthquakes, for example, the 1964 Alaska, 1969 Santa Rosa, and 1971 San Fernando earthquakes. However, until now there have been no destructive field vibration tests of repaired buildings to determine their ability to sustain future earthquake excitations.

Laboratory cyclic tests[1,2] conducted at the University of California, Berkeley (UCB), have shown that the epoxy-injection technique is quite effective in restoring the original strength and energy-absorption characteristics of structural components, such as rectangular reinforced concrete beams and columns. However, these subassembly tests have revealed that the technique is only partially successful in recovering original stiffness. In a paper reviewing cyclic loading tests of epoxy-repaired subassemblies at UCB and other laboratories, Popov and Bertero[3] concluded that a repaired structure may be 2 to 2.5 times more flexible than the original, undamaged structure. They noted that forced-vibration field tests of a structure in both its original and repaired states would be very valuable in relating the results of cyclic tests of subassemblies to the behavior of actual structures.

Shaking-table tests have been conducted at UCB on two reinforced concrete frame models in both their original and epoxy-repaired states.[4,5] The models were seven-tenths scale and represented 2-story structures. These

tests provided results similar to the cyclic subassembly tests by indicating the effectiveness of the epoxy-injection technique in recovering the strength and energy-absorption properties of the original structures but showing that it was not capable of recovering all of the stiffness lost because of damage.

One of the 4-story reinforced concrete structures at the Nevada Test Site (NTS) offered the ideal opportunity for further dynamic testing of a full-scale structure because it had been repaired by the epoxy-injection method.

4-Story Reinforced Concrete Test Structures

In 1965, two identical 4-story reinforced concrete structures were designed and constructed at the NTS specifically for field investigations associated with a structural response program conducted by URS/John A. Blume & Associates, Engineers (URS/Blume), for the U.S. Atomic Energy Commission (now the U.S. Department of Energy). These test structures are 12 ft by 20 ft, centerline to centerline, in plan with 9-ft story heights. Each structure consists of four reinforced concrete floor slabs with perimeter beams supported by four corner columns.

The design of the structures was consistent with the 1963 edition of the American Concrete Institute (ACI) building code requirements.[6] Design for lateral loads was based on seismic requirements of the 1961 *Uniform Building Code (UBC)*[7] for Seismic Zone 3. Some provisions for ductility and reserve energy-absorption capacity[8,9] were also incorporated into the design of the structure. Thus, the ductility of the structures conforms to the thinking on that subject at the time of design but does not completely conform to current code requirements.

In the determination of the design lateral force according to the 1961 *UBC* requirements for Seismic Zone 3, the weight of each floor included 100 psf live load in addition to the dead load of the bare frame. This accounted for the additional weight of the testing equipment and nonstructural partitions that would be present during various tests. Since the dead load was approximately 100 psf, the design lateral force was nearly twice that necessary to satisfy the Seismic Zone 3 requirements of the 1961 *UBC* if only

the bare frame was considered. However, the design lateral force is approximately equal to the force needed to satisfy the Seismic Zone 4 requirements of the 1982 *UBC*,[10] considering only the bare frame.

History of the Testing Program

Between 1966 and 1973, the two structures were subjected to ground motions caused by more than 50 underground nuclear explosions and to numerous nondestructive vibration tests, in which the vibrations were created by pull-release, vibration generator, and human-induced methods. In order to study the effects of nonstructural partitions on structural response, various types of partitions were added to the structures for some of these tests. The vibrations created by these tests (with the possible exception of one) were all of relatively low amplitude; the structural frames were thus not damaged, although, in some instances, partitions showed minor damage. It is possible that ground motions produced by one particular underground nuclear explosion may have caused yielding of some of the reinforcing steel. Results of these tests and associated analyses are described in several reports[11-14] and technical papers.[15,16]

In 1974, one of the structures was deliberately forced into the range of inelastic response by means of a reciprocating-mass vibration generator. The principal purposes of this testing were to compare theoretical nonlinear response predictions with actual recorded response and to determine the character of the onset of structural damage for reinforced concrete structures. Structural damage was extensive, consisting of x-cracking and spalling at beam-column connections. The type and extent of the damage were similar to what might be expected from a major earthquake. Results from the 1974 testing program were published in report form in 1976[17] and were presented at the Sixth World Conference on Earthquake Engineering[18] and the 1976 ACI International Conference on Concrete Structures.[19]

In June 1975, the damaged structure was repaired by the epoxy-injection technique. The repair work, which used a patented repair process,[20] represented typical postearthquake repairs. The repaired structure provided an excellent opportunity to determine the effectiveness of epoxy-injection techniques in recovering the original physical properties of structures.

Since testing of an epoxy-repaired structure would be beneficial to the earthquake engineering community, the National Science Foundation (NSF) funded the testing and analysis reported here. Retesting took place in September 1979. This report describes the retest procedures and the results of the analysis and compares the results with those of previous tests.

Funding for this project was provided by the NSF under Agreement CEE-7812714. DOE's Nevada Operations Office (DOE-NV) provided the repaired structure, strong-motion instrumentation, and administrative support.

2. DESCRIPTION OF ESSENTIAL EQUIPMENT

The Test Structure

The reinforced concrete test structure is 12 ft by 20 ft, centerline to centerline, in plan with four 9-ft stories (see Figure 1). The floors are supported by four rectangular corner columns, 16 in. by 14 in. The floor slabs are 6 in. thick and are reinforced for two-way action. Spandrel beams around the perimeter of each floor slab are 16 in. by 15 in. in the 20-ft direction and 14 in. by 12 in. in the 12-ft direction. Details of the placement of reinforcing steel are provided in another URS/Blume report.[11]

Tests of concrete cylinders indicated 28-day compressive strengths ranging from 4,000 to 5,000 psi.[11] Tests of reinforcing steel coupons showed yield strengths between 45,000 and 55,000 psi and ultimate strengths at approximately 90,000 psi.[11] For the purposes of analysis in this study, concrete compressive strength is taken to be 4,500 psi, and yielding of the reinforcing steel is taken to be 50,000 psi.

Prior to the 1974 tests, a 3-ft-thick concrete pad was poured onto the existing ground floor slab to prevent overturning during the destructive test. This pad was in place for the 1979 tests as well. A 2-in. gap between the concrete pad and the columns prevented contact between the pad and the columns during the testing.

The test structure was deliberately damaged by forced vibrations in the 1974 test program. A year later, the structure was repaired by injection of a high-strength epoxy compound into all significant cracks. A sealer was first used to cover each crack, leaving gaps at selected locations to serve as injection and relief ports. When the sealer had set, the epoxy compound was injected into the cracks at the injection ports until it was expressed at the relief ports. The sealer was sanded off after the epoxy had hardened.

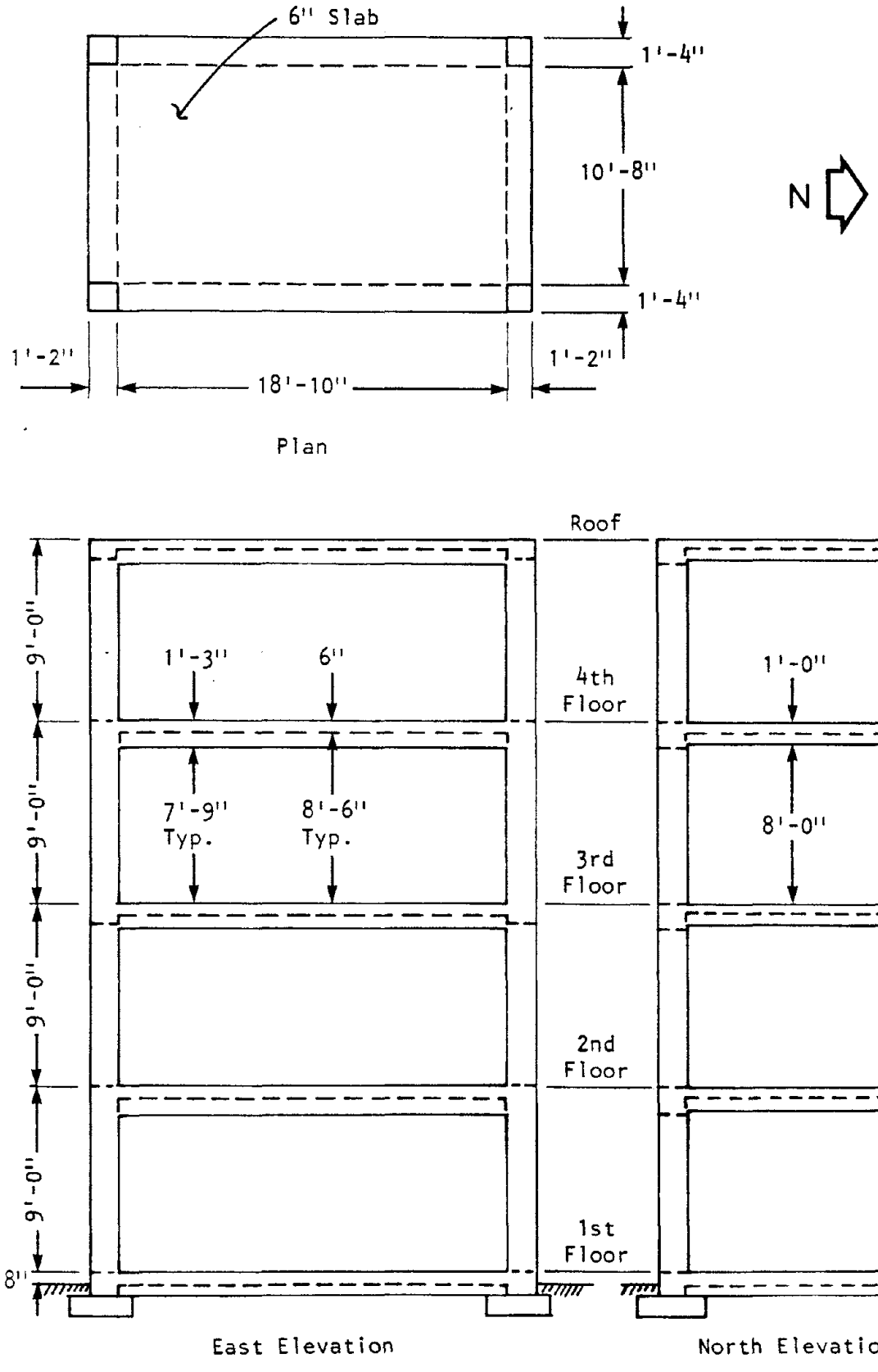

FIGURE 1 4-STORY CONCRETE TEST STRUCTURE

The Vibration Generator

The same vibration generator used in the 1974 tests of the original structure was used in the 1979 tests of the epoxy-repaired structure. The generator used a hydraulic piston to move a large reaction mass through reciprocating motion, thereby creating an oscillating driving force on the structure. This apparatus was designed and assembled by Sandia National Laboratories (Sandia), Albuquerque, New Mexico. Figures 2 and 3 show the vibrator in place on the structure.

The reaction mass is supported by four V-groove casters that move on tracks on the top of a supporting frame. This frame, constructed from two 12-in. wide-flange beams, distributed the weight of the reaction mass over a large portion of the floor. The weight of the supporting frame is approximately 4,000 lb. In 1974, the reaction mass consisted of a 10-in.-thick steel plate weighing 15,000 lb. The same reaction mass was used for most of the 1979 tests; however, for several of the tests, the inclusion of additional steel plates increased the weight of the reaction mass to 24,500 lb.

The hydraulic piston had a maximum displacement of 3.9 in. from zero to peak, or nearly 8 in. peak to peak. A displacement gauge measured the displacement of the oscillating mass relative to the supporting frame. The force in the hydraulic piston was measured by a strain-gauge-type force transducer mounted between the piston and the supporting frame. The control system would maintain the force in the piston at some prescribed value and at some prescribed frequency.

The friction in the wheel bearing created a force opposing the motion of the reaction mass relative to the floor. Chen et al.[17] estimated this friction force to be 1% of the deadweight of the mass on the basis of the manufacturer's rating of the wheel bearings. This value seemed reasonable in comparison with the amount of force required to initiate vibrations in the 1974 tests. In the 1979 tests, the force required to initiate vibration was somewhat higher, in part because of the increased age of the system and in part because of heavier reaction mass. For purposes of analysis in this study, the friction force was estimated to be 1% of the deadweight when the lighter reaction mass was used and 1.5% when the heavier mass was used.

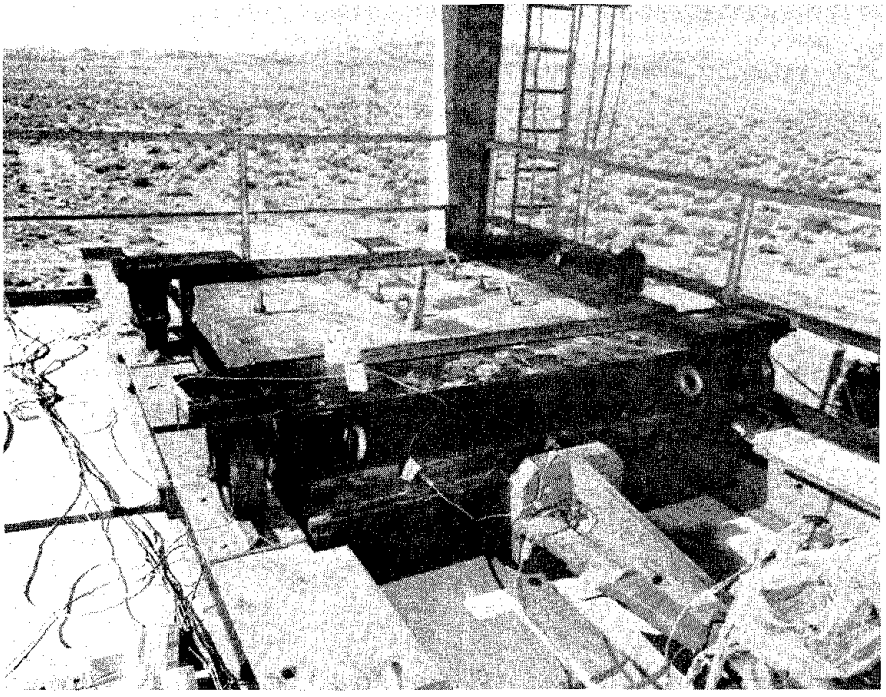

FIGURE 2 VIBRATION GENERATOR IN PLACE ON THE TEST STRUCTURE

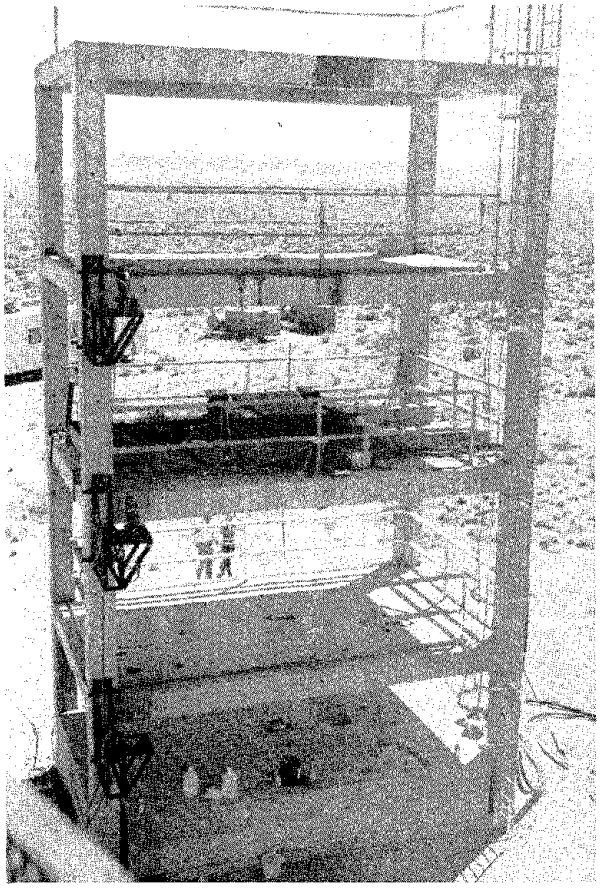

FIGURE 3 VIBRATION GENERATOR ON THE THIRD FLOOR OF THE TEST STRUCTURE

The vibration generator and associated hardware are described in more detail by Chen et al.[17] and by Smallwood and Hunter.[21]

Instrumentation

Seismograph System. The network of motion transducers placed on the building to monitor structural response during the tests consisted of L-7 velocity meters and Sunstrand accelerometers. The L-7 seismograph system is a compact, versatile unit capable of recording on magnetic tape as well as on paper strip charts over a range of velocity from 100 cm/sec to 9×10^{-5} cm/sec. The L-7 seismometer has a natural frequency of 1.875 Hz with 10 times critical damping. The seismometer output is proportional to acceleration, and the seismometer amplifier has a frequency response inversely proportional to the seismometer response. Thus, the resulting electrically integrated signal output from the amplifier is proportional to the velocity and is flat over the frequency range of 0.1 Hz to 30 Hz. The attenuation capability of the amplifier ranges from -60 dB to +60 dB in 6-dB steps. The signal-to-noise ratio is 40 dB minimum for all attenuator settings from -60 dB to +42 dB. A detailed description of the L-7 seismograph system can be obtained from Navarro and Wuollet.[22]

Because the Q-Flex accelerometers used in the instrumentation of the 1974 tests were unavailable, Sunstrand accelerometers were used as duplicate instrumentation for the structure. These two brands of accelerometers have similar specifications, although their internal circuitry is different. The Sunstrand has a range of 0.5g to 40.0g. With adjustments made according to Sunstrand specifications, the accelerometer range was changed to 0 to 1.0g and calibrated for positive and negative 1.0g accelerations. However, because the magnetic tape recorder specifications were incompatible with the instrument specifications, the negative 1.0g calibrations could not be recorded properly.

Ten L-7 velocity meters measured the principal structural responses during each test at locations and in the directions indicated in Figures 4, 5, and 6. Figures 4 and 5 represent the configurations used in the nondestructive tests with forced vibrations in the 12-ft direction (transverse) and the 20-ft direction (longitudinal), respectively. Figure 6 represents the

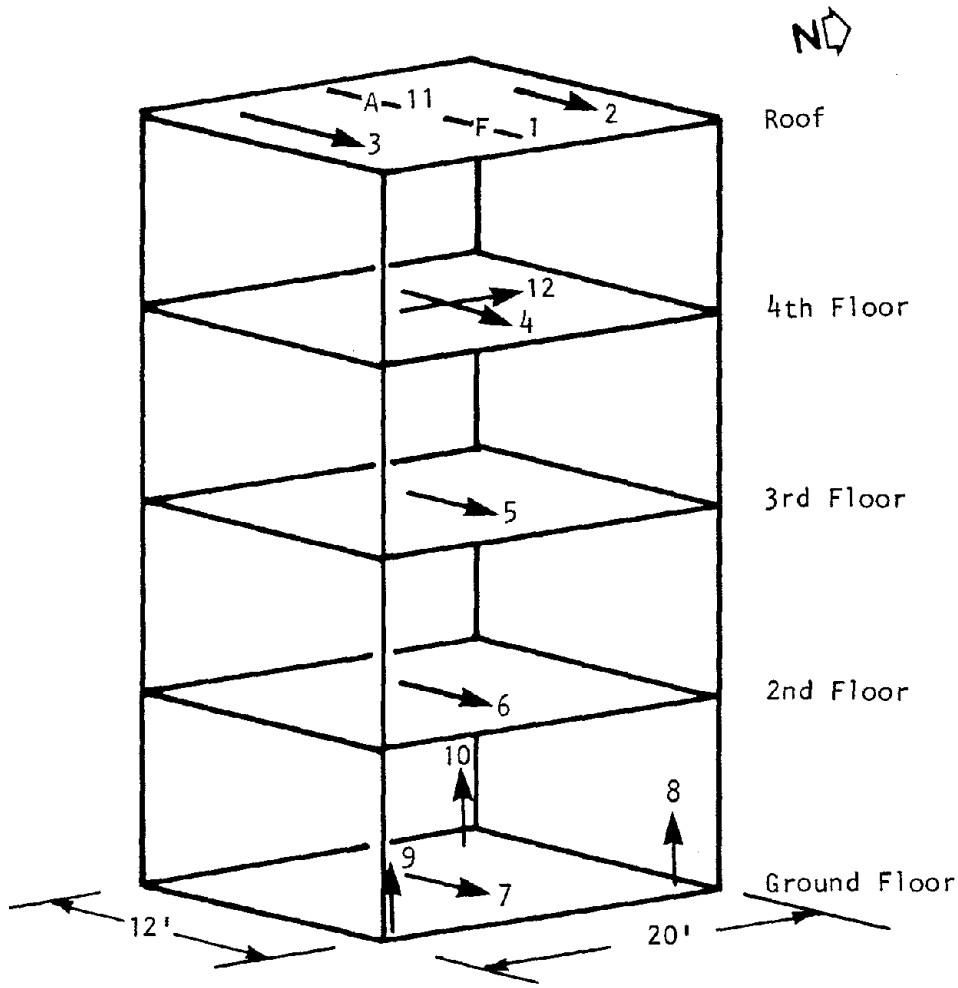

FIGURE 4 INSTRUMENT LOCATIONS AND AXIAL ORIENTATIONS FOR NONDESTRUCTIVE TESTS, TRANSVERSE DIRECTION

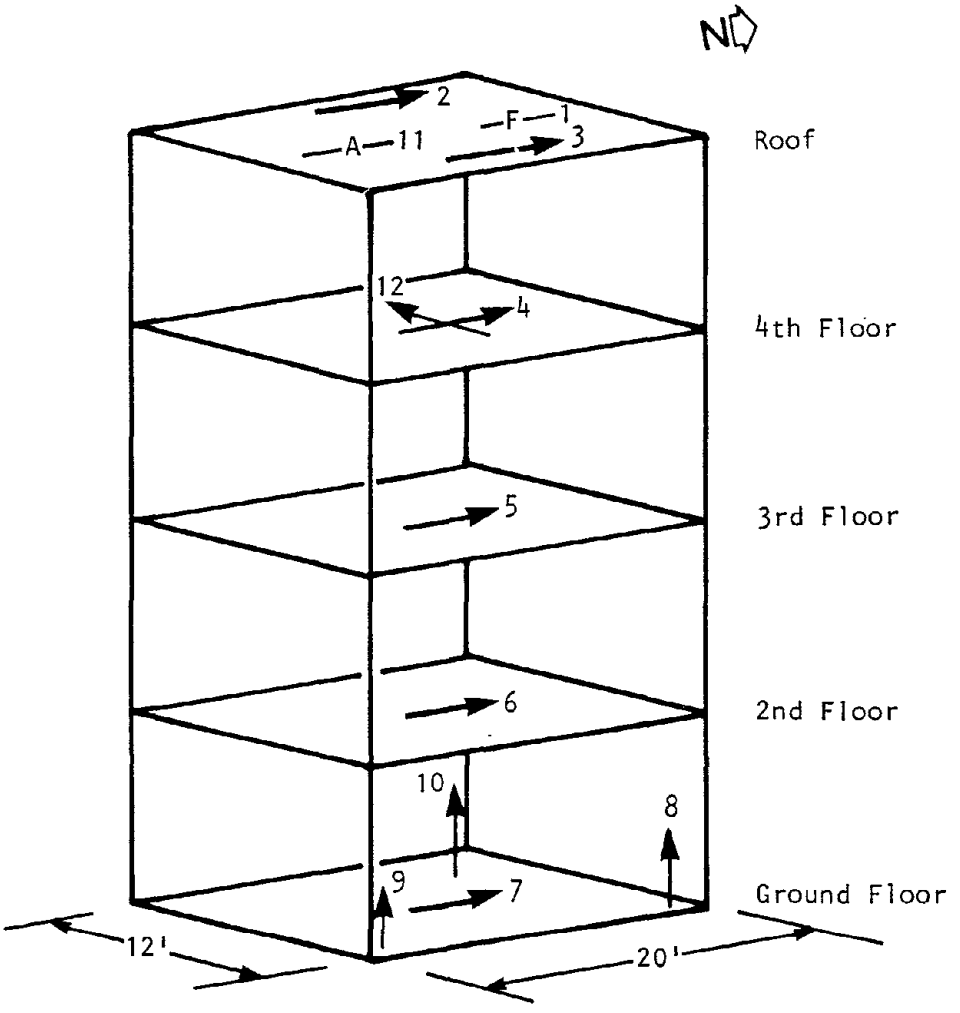

Symbols:
—F— Force transducer
—A— Reaction mass accelerometer
→ Seismometer

FIGURE 5 INSTRUMENT LOCATIONS AND AXIAL ORIENTATIONS FOR NONDESTRUCTIVE TESTS, LONGITUDINAL DIRECTION

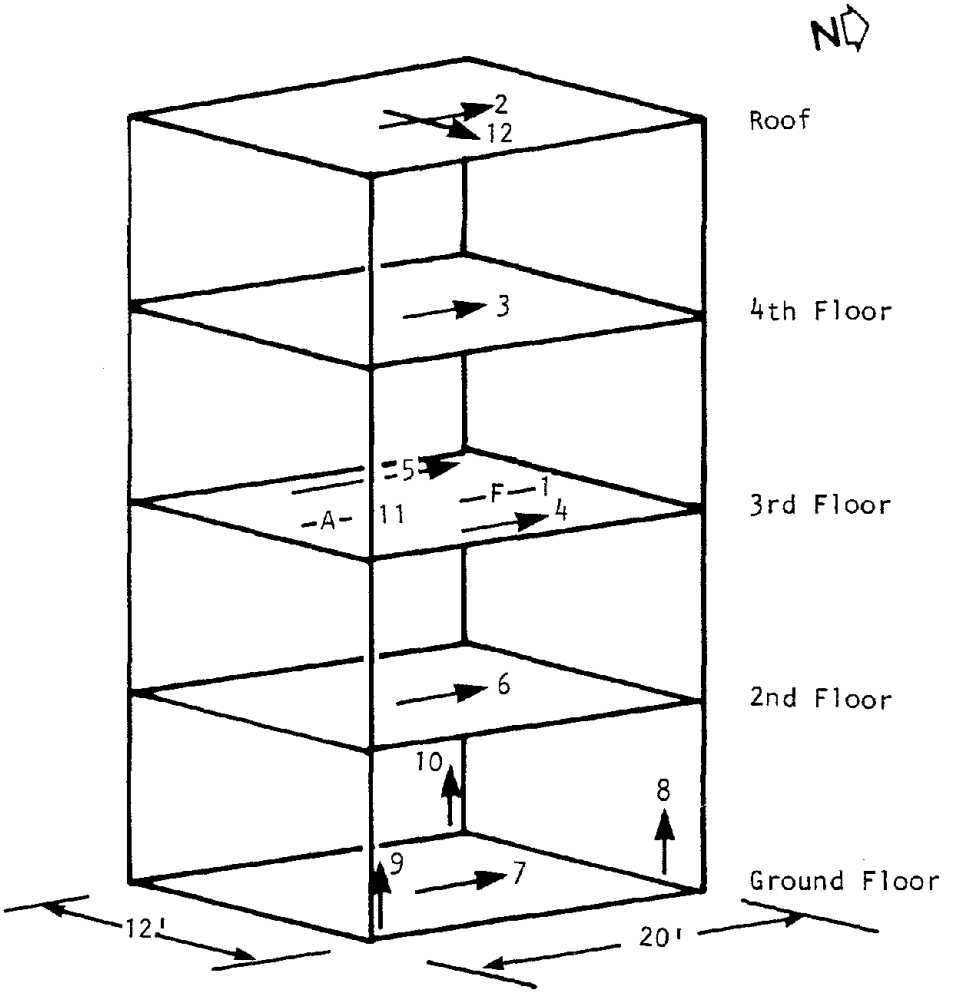

Symbols:
- —F— Force transducer
- —A— Reaction mass accelerometer
- ⟶ Seismometer

FIGURE 6 INSTRUMENT LOCATIONS AND AXIAL ORIENTATIONS FOR DESTRUCTIVE AND POSTDESTRUCTIVE TESTS

arrangement used in the destructive and postdestructive tests, where the forced vibrations were in the longitudinal direction only. These configurations were duplicated with the accelerometers. In addition to these seismometers, the seismograph system included the force transducer, which measured the force between the vibration generator and the building, and a Sunstrand accelerometer mounted on the reaction mass.

These arrangements of seismometers permitted the measurement of horizontal motions of all floors and the rocking motion of the ground floor in the direction of the input force. In addition, the torsional motion of the floor where the vibration generator was mounted could be monitored. The horizontal seismometer represented by instrument number 12 in Figures 4 through 6 provided a measure of the motion in the direction perpendicular to the direction of the force.

A 14-channel recording system was used to record the force transducer signal and the reaction mass acceleration on magnetic tape simultaneously with the velocities from the 10 L-7 velocity meters. The IRIG-E time code and the FM compensation were recorded on the remaining two channels. The assignments of the 14 channels on the magnetic tapes are listed in Tables 1, 2, and 3 for the various test series. In addition to recording these signals on magnetic tape, they were also recorded on paper strip charts in real time during the test.

Another 14-channel recording system was used to record the signals from the Sunstrand accelerometers, located on the floors, simultaneously with the reaction mass acceleration signals. The force transducer signal was not recorded on this system. The data were recorded on magnetic tape only and not on paper strip charts. This system provided duplication so that accidental loss of one set of data would not cause a total loss of response information.

An additional seismometer network was buried a few inches below the ground surface to measure transmission of vibrations away from the structure through the soil. Twelve L-7 velocity meters were placed, with three at each of four locations: on the ground floor and at 5 ft, 30 ft, and 60 ft away from the building. A set of three seismometers measured vibrations in

TABLE 1

RECORDING CHANNELS FOR NONDESTRUCTIVE TESTS

IN THE TRANSVERSE DIRECTION

Channel	Instrument	Contents*
1	1	Force transducer
2	2	Velocity, roof, north side
3	3	Velocity, roof, south side
4	4	Velocity, fourth floor
5	5	Velocity, third floor
6	6	Velocity, second floor
7	7	Velocity, ground floor
8	8	Velocity, vertical, NE corner
9	9	Velocity, vertical, SE corner
10	—	FM compensation
11	10	Velocity, vertical, NW corner
12	11	Acceleration, vibration generator reaction mass
13	12	Velocity, fourth floor, longitudinal
14	—	IRIG-E time code

*Directions are transverse unless otherwise noted.

TABLE 2

RECORDING CHANNELS FOR NONDESTRUCTIVE TESTS

IN THE LONGITUDINAL DIRECTION

Channel	Instrument	Contents*
1	1	Force transducer
2	2	Velocity, roof, west side
3	3	Velocity, roof, east side
4	4	Velocity, fourth floor
5	5	Velocity, third floor
6	6	Velocity, second floor
7	7	Velocity, ground floor
8	8	Velocity, vertical, NE corner
9	9	Velocity, vertical, SE corner
10	—	FM compensation
11	10	Velocity, vertical, NW corner
12	11	Acceleration, vibration generator reaction mass
13	12	Velocity, fourth floor, transverse
14	—	IRIG-E time code

*Directions are longitudinal unless otherwise noted.

TABLE 3

RECORDING CHANNELS FOR DESTRUCTIVE AND POSTDESTRUCTIVE TESTS

Channel	Instrument	Contents
1	1	Force transducer
2	2	Velocity, roof
3	3	Velocity, fourth floor
4	4	Velocity, third floor, east side
5	5	Velocity, third floor, west side
6	6	Velocity, second floor
7	7	Velocity, ground floor
8	8	Velocity, vertical, NE corner
9	9	Velocity, vertical, SE corner
10	11	Acceleration, vibration generator reaction mass
11	10	Velocity, vertical, SW corner
12	—	FM compensation
13	12	Velocity, roof, transverse
14	—	IRIG-E time code

the two horizontal directions (longitudinal and transverse to the structure) and the vertical direction. Seismometer locations for the various tests are indicated in Figures 7 and 8. The signals from this network were recorded on magnetic tape, along with the FM compensation and the IRIG-E time code.

Photographic Coverage. Six motion picture cameras were installed to provide permanent documentation of the damage done to the structure during the destructive test. Four cameras were mounted on the test structure as shown in Figure 9, and one was located about 100 ft away from the structure to record overall motion of the structure. The sixth camera was a roving unit used to capture close-up views of various parts of the structure during the destructive test. In addition to motion pictures, many still photographs were taken before and after the destructive test.

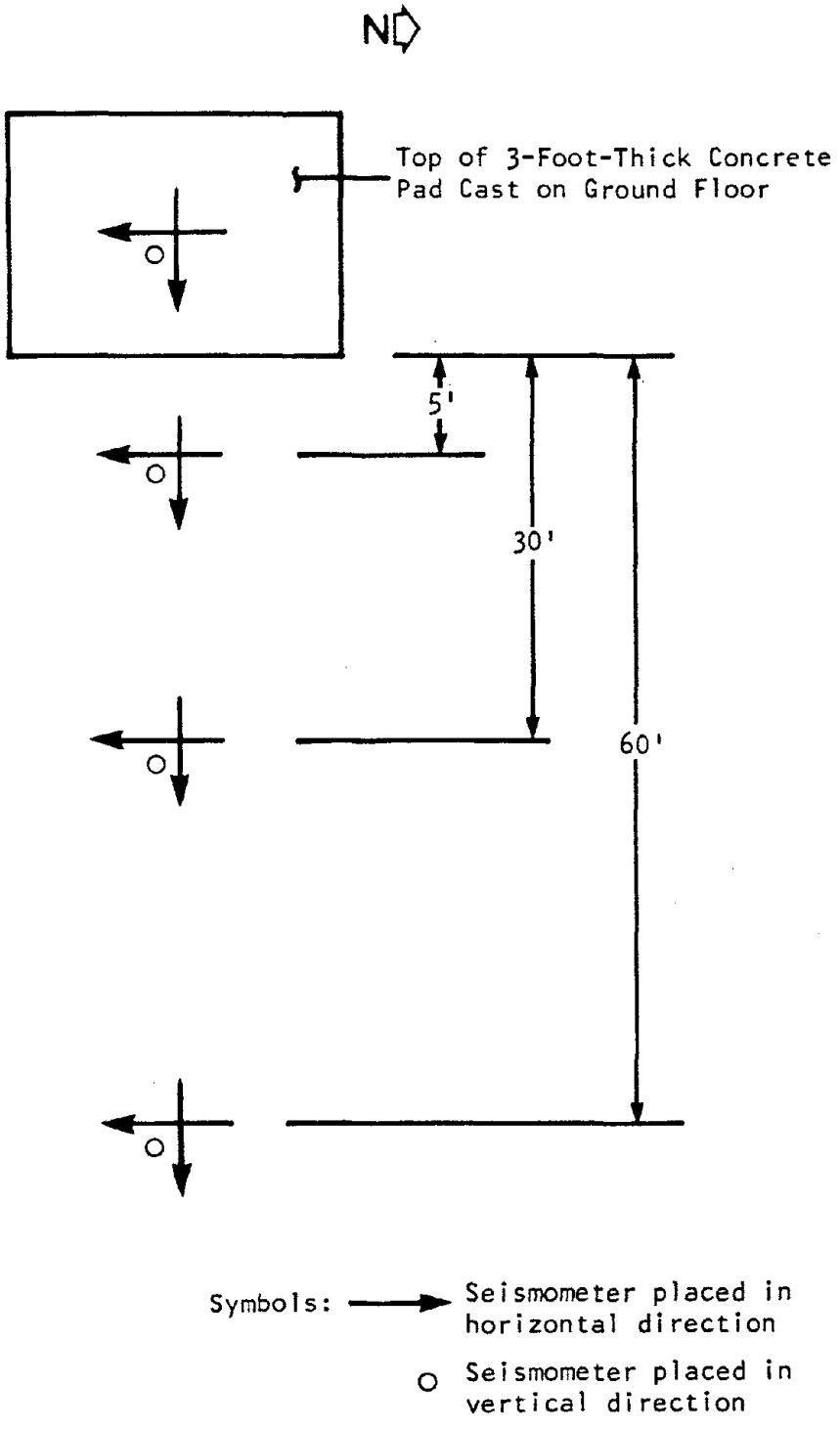

FIGURE 7 GROUND SURFACE INSTRUMENTATION FOR NONDESTRUCTIVE TESTS, TRANSVERSE DIRECTION

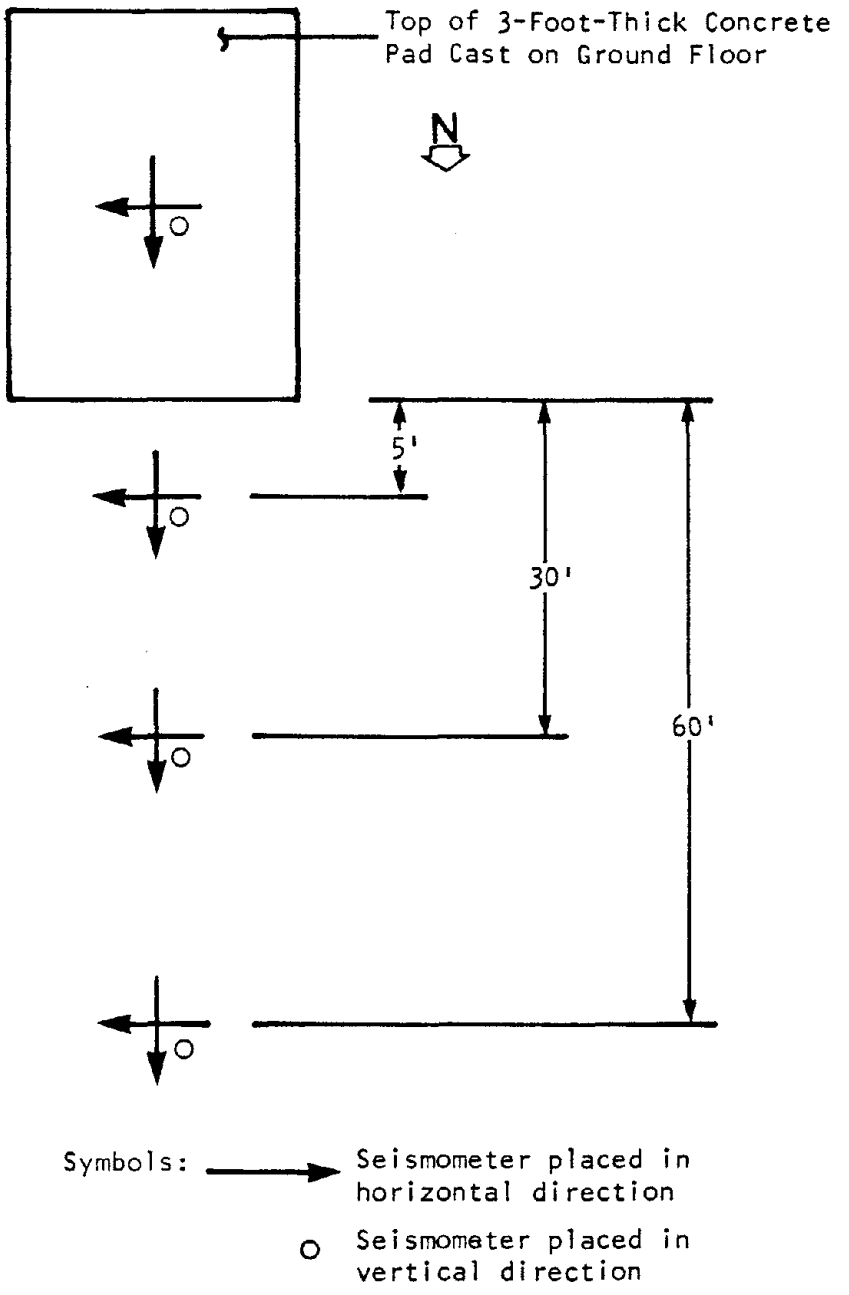

FIGURE 8 GROUND SURFACE INSTRUMENTATION FOR ALL TESTS IN THE LONGITUDINAL DIRECTION

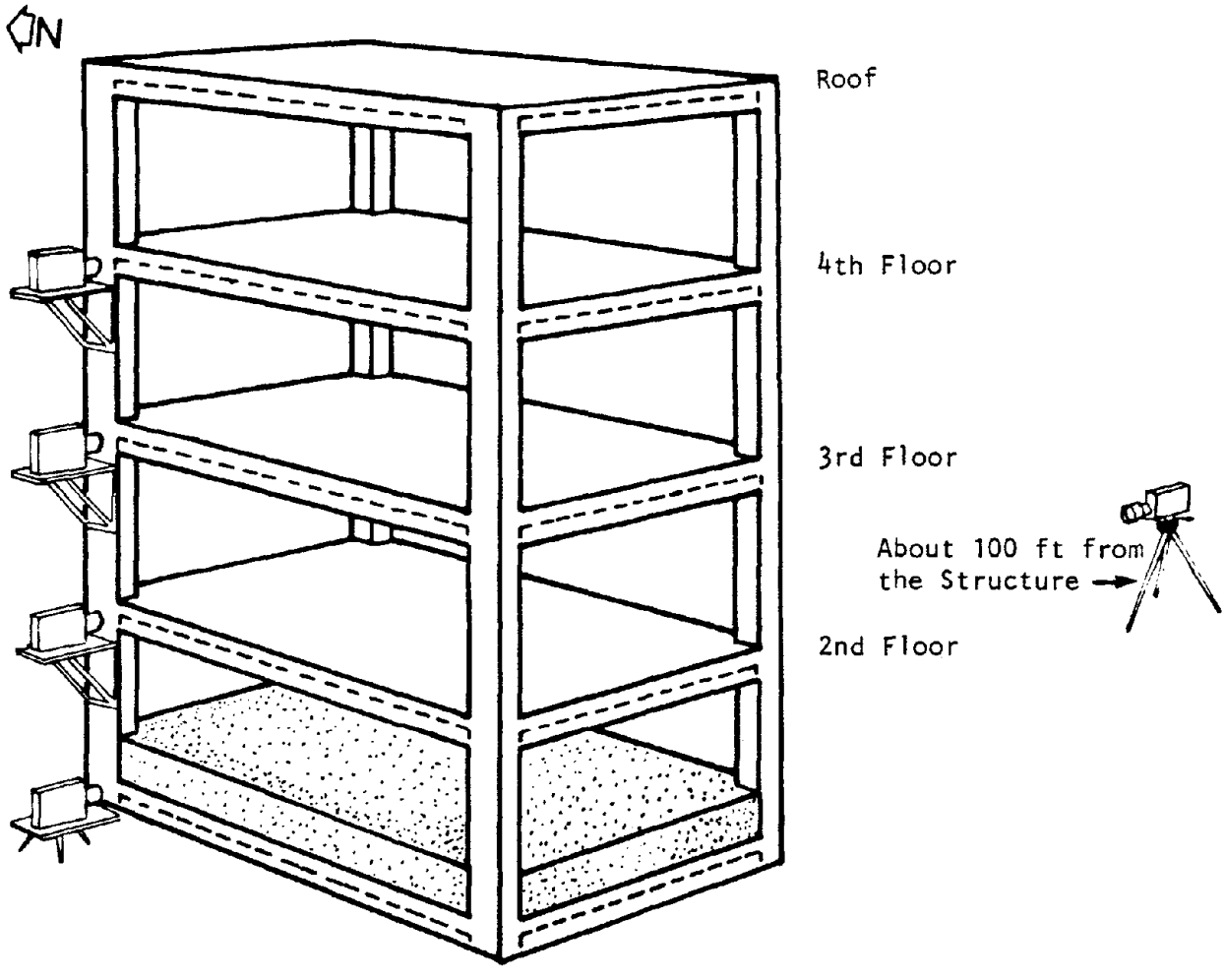

Note: An additional camera moved from place to place.

FIGURE 9 PLACEMENT OF MOTION PICTURE CAMERAS ON THE TEST STRUCTURE

3. DESCRIPTION OF TEST PROCEDURES

The 1979 test procedures for the epoxy-repaired structure were almost identical to the procedures followed in the 1974 tests of the original structure. Nondestructive testing (Test Series OE) was conducted first. In that series, the vibration generator was located on the roof, and the building was shaken in both the longitudinal (north-south) and transverse (east-west) directions. Destructive testing (Test Series PE) was performed in the longitudinal direction with the vibration generator on the third floor. Postdestructive testing (Test Series QE) was conducted with the vibration generator on the third floor and at force levels similar to those used in the nondestructive tests. These tests are described in detail in the sections below.

In the 1974 tests, these three test series were identified by the letters O, P, and Q, respectively. In the 1979 tests, the same identifiers were used with the addition of the letter E to signify that the test was conducted on the epoxy-repaired structure. In 1979, a new series of tests, designated Test Series IE, was added to the test program to investigate the interaction between the vibration generator and the structure. There was no corresponding test series in the 1974 test program.

To distinguish individual tests within a test series, additional numbers and letters were employed. Identifiers for tests that dwell on a particular modal frequency begin with the letter M; identifiers for frequency sweep tests begin with a number. The notations 1-T-OE and 1-L-OE identify the first frequency sweep tests in the transverse and longitudinal directions, respectively. A number 2 in place of the number 1 means that the dwell frequency corresponds to mode 2, and so on. The notation is also followed in the other test series.

Pretest Condition of the Structure

The concrete test structure was visually inspected before any testing was conducted. Hairline cracks in beams, columns, and slabs were visible at all floor levels. These cracks were probably the unrepaired cracks from previous testing. Epoxy-repaired cracks were not clearly visible, probably

because the epoxy on the concrete surface had been ground off following the repairs and because of subsequent weathering of the surface. A few new cracks were observed at the location of epoxy-repaired cracks; however, it was not clear whether these cracks were on the surface or penetrated into the concrete.

Nondestructive Tests

Nondestructive tests were conducted prior to the destructive test in order to study the structural response at small motion amplitudes where the structure was expected to exhibit approximate linear elastic behavior. The vibration generator was mounted on the roof slab, oriented first to create motion in the transverse direction. After conducting a sequence of tests with the vibration generator in that orientation, the vibration generator was rotated 90° to create motion in the longitudinal direction, and the test sequence was repeated. The weight of the reaction mass for the nondestructive tests was 15,400 lb (7,000 kg).

The first tests to be conducted in each direction were a series of frequency sweep tests to locate the modal frequencies. The procedure was to sweep the driving frequency across a specific frequency range while maintaining the force at a specified value. Most sweep tests began at 0.5 Hz or 1.0 Hz and extended to 30 Hz, although several began at about 10 Hz. The vibration generator did not operate accurately at low amplitudes and low frequencies; therefore, many sweep tests began with manual control of the frequency and were stopped at 4 Hz to transfer controls from manual to automatic. Whether manual or automatic, the control of the frequency was such that there was an approximately equal number of cycles for an equal percentage increase in frequency.

Following the sweep tests for a particular direction, modal dwell tests were conducted for that direction. The test structure was vibrated in one of the four lowest modal frequencies identified in the sweep tests. While the driving frequency was maintained at the prescribed value, the driving force was increased in increments with sufficient time lapse between increases to permit the response to reach steady-state conditions.

The various nondestructive tests are identified in Table 4. The values for force and frequency are those indicated in the field logs.

Vibration Generator—Structure Interaction Tests

Following the nondestructive tests, a series of tests was conducted to investigate the interaction between the vibration generator and the structure and to study the effects of the magnitude of the reaction mass on system performance. The vibration generator was located on the roof, oriented in the longitudinal direction. Some of the tests were conducted with the initial reaction mass of 15,400 lb (7,000 kg). Other tests were conducted with one or two additional masses weighing approximately 4,500 lb (2,000 kg) each. With the first additional mass placed on top of the initial mass, the reaction mass weighed 20,000 lb (9,060 kg). With both additional masses on the initial mass, the total weight was 24,500 lb (11,100 kg).

Frequency sweep tests and modal dwell tests were conducted in a similar manner to the previous nondestructive tests but with increased reaction mass. In addition, a series of low-amplitude tests was conducted in which the forcing frequency was kept constant at preselected frequencies regardless of the structural response motions. Specifications for these tests are given in Table 5.

Destructive Test

Following the interaction tests, the vibration generator was moved to the third floor and oriented in the longitudinal direction for the destructive test series. This location duplicated the arrangement used in the 1974 tests. A parameter study conducted prior to the 1974 tests had identified this location as the optimum position for shaking the structure for the destructive test.[17]

The destructive test began with low-amplitude vibrations at the building's fundamental period for that level of motion. The force level was increased in predetermined increments with accompanying adjustments to the forcing frequency to keep the frequency as close as possible to the resonant frequency of the first mode. This procedure was continued until the motion of the reaction mass relative to its supporting frame reached its limit. At

TABLE 4

INPUT DATA FOR NONDESTRUCTIVE TESTS

Frequency Sweep Tests

Sweep Test Number	Force (lb)	Frequency Range (Hz)
1-T-OE	200	0.5-30
2-T-OE	400	0.5-30
3-T-OE*	600	0.5-30
4-T-OE	1,200	5-30
5-T-OE*	2,000	5-30
6-T-OE	4,000	10-30
7-T-OE*	8,000	10-30
1-L-OE	200	NA
2-L-OE*	400	1-40
3-L-OE*	800	1-30
4-L-OE	1,500	4-30
5-L-OE*	2,500	4-30
6-L-OE	4,000	9-30
7-L-OE*	8,000	9-30

Frequency Dwell Tests*

Dwell Test Number	Force (lb)	Approximate Frequency (Hz)
M-1-T-OE	60	1.8
M-2-T-OE	400-1,000	7.1
M-3-T-OE	400-6,000	13.6
M-4-T-OE	500-8,000	21.0
M-1-L-OE	800	1.9
M-2-L-OE	500-2,500	6.0
M-3-L-OE	1,000-8,000	10.4
M-4-L-OE	? -8,000	?

*Structural response data from velocity meters have been digitized.

†Test 1-L-OE was canceled because the system would not function at the specified force level.

TABLE 5

INPUT DATA FOR VIBRATION GENERATOR–STRUCTURE INTERACTION TESTS

Frequency Sweep Tests

Sweep Test Number	Reaction Mass Weight (lb)	Force (lb)	Frequency Range (Hz)
1-L-1E*	20,000	400	1–30
2-L-1E*	20,000	800	1–30
3-L-1E	24,500	600	1–30
4-L-1E*	24,500	800	1–30

Frequency Dwell Tests

Dwell Test Number	Reaction Mass Weight (lb)	Force (lb)	Frequency (Hz)
5-L-1E	20,000	400	1.75
6-L-1E*	20,000	800	1.75
7-L-1E	24,500	600	2.8
8-L-1E*	24,500	800	2.2

Constant-Frequency Tests*

Test Number	Reaction Mass Weight (lb)	Force (lb)	Frequency (Hz)
9-L-1E	15,400	400	1.8
10-L-1E	15,400	400	2.2
11-L-1E	15,400	400	5.9
12-L-1E	15,400	400	7.2
13-L-1E	20,000	400	1.8
14-L-1E	20,000	400	2.2
15-L-1E	20,000	400	5.9
16-L-1E	20,000	400	7.2
17-L-1E	24,500	400	1.8
18-L-1E	24,500	?	2.2
19-L-1E	24,500	400	5.9
20-L-1E	24,500	400	7.2

*Structural response data from velocity meters have been digitized.

the termination of the destructive test, the structure had suffered extensive damage; however, the damage was not as extensive as that caused by the 1974 test.

The procedures used in the destructive test of the epoxy-repaired structure differed in two aspects from those used in the 1974 test of the original structure. First, the reaction mass included the two additional masses; therefore, the reaction mass weighed 24,500 lb and not 15,400 lb as in 1974. This increase in the weight increased the gravity load forces in the third floor and in the columns below the third floor. This had the effect of decreasing the bending moment capacity of the third-floor beams and increasing the stiffness of the columns below the third floor. Other effects of the increased reaction mass are unknown.

The second difference in testing procedures was that the test was manually controlled. During the 1974 destructive test, the automatic controlling system was unable to maintain the driving frequency at the resonant frequency of the structure. As the force level was increased, the properties of the structure would change, characterized in particular by a lengthening of the fundamental period. The automatic controls would attempt to track the changing period by maintaining the phase angle between the floor acceleration and the force transducer signals at 90°. However, the controls were unable to track this change properly, and the response would drop to low-amplitude motion. This phenomenon was attributed to the double-value characteristics of the frequency response curves for a nonlinear structure at driving frequencies adjacent to the resonant frequency of the structure.[17] To prevent this situation in the 1979 destructive test, it was decided to maintain the phase angle at 120°, slightly above resonant conditions. The vibrator force was manually increased in increments, and the frequency was manually adjusted as needed to maintain the phase angle at 120°.

The destructive test was preceded by a sweep test to confirm the resonant frequency and to check the equipment. The tests in Test Series PE are identified in Table 6.

TABLE 6

INPUT DATA FOR THE DESTRUCTIVE TEST

Nondestructive Frequency Sweep Test

Sweep Test Number	Constant Force (lb)	Frequency (Hz)
1-L-PE	1,000	1-30

Destructive Frequency Dwell Test

Dwell Test Number	Force (lb)	Frequency (Hz)
M-1-L-PE	500-6,000	Varied

Note: Structural response data from velocity meters have been digitized.

Postdestructive Tests

The primary objective of the postdestructive tests was to observe the behavior of the damaged structure at values of motion amplitudes corresponding to the original elastic range. The procedures followed were similar to those used in the nondestructive tests, except that the vibration generator was located on the third floor instead of on the roof and oriented only in the longitudinal direction. This test series consisted of a single frequency sweep test, to survey modal frequencies, followed by modal dwell tests. The various postdestructive tests are identified in Table 7.

Data Collection and Storage

The motions of the structure were measured by L-7 velocity meters and Sunstrand accelerometers, as described in the section on instrumentation. Signals were recorded on magnetic tape in analog form by three separate recording systems. One system recorded the signals from the 10 L-7 velocity meters located on the structure simultaneously with the signals from the force transducer and reaction mass accelerometer. The signals from the 10 accelerometers were recorded simultaneously with the reaction mass accelerometer signal by another recording system. A third system recorded the signal from the 12 L-7 velocity meters in the ground surface instrumentation array.

These three separate tape recordings were made for each test with the exception of the destructive test. Just prior to the start of destructive testing, a temporary power cutoff caused the accelerometer recorder to shut off. When the power was restored, the recorder did not automatically turn on, and the accelerometer data for the destructive test were not recorded on magnetic tape. However, the data from the other two networks were recorded for the destructive test.

Following the tests, the magnetic tapes were transferred to the Las Vegas office of URS/Blume for permanent storage. Duplicate tapes were made and sent to Sandia offices at Mercury, Nevada, for digitization.

TABLE 7

INPUT DATA FOR THE POSTDESTRUCTIVE TEST

Frequency Sweep Test

Sweep Test Number	Constant Force (lb)	Frequency (Hz)
1-L-QE	1,000	1-30

Frequency Dwell Tests

Dwell Test Number	Force (lb)	Frequency (Hz)
M-1-L-QE	800	1.7
M-2-L-QE	2,500	5.0
M-3-L-QE	8,000	11.3
M-4-L-QE	8,000	14.2

Note: Structural response data from velocity meters have been digitized.

The motion pictures and still photographs, which were recorded by Pan American World Airways, DNA Photo Project (Pan Am), were transferred to the Pan Am offices at Mercury, Nevada, for development and storage. Prints were sent to the San Francisco office of URS/Blume for evaluation.

4. ANALYSIS OF RESPONSE DATA

Data Digitization

A significant amount of data were collected in this testing program. It was not practical to digitize all recorded data; therefore, only specific tests were selected for digitization. All frequency dwell tests and some of the frequency sweep tests were selected. The vibration generator—structure interaction tests were also digitized, although there were no plans to analyze these test data in this study. The tests that were digitized are indicated in Tables 4 through 7.

The structural responses were measured by both velocity meters and accelerometers in all tests except the destructive test. As discussed earlier, a malfunction of the accelerometer recording system prior to the destructive test resulted in the loss of the accelerometer data in that test. In order to use structural response data from the same origin for all tests, it was decided to digitize only the response data measured by the L-7 velocity meters.

Before digitizing test data, the original magnetic tapes were played back and the signals recorded on paper strip charts. The quality of the data was then evaluated by visually inspecting the paper strip charts. During this process, it was discovered that the ground motion data — measured by the array of 12 L-7 velocity meters on the ground floor and at various distances from the structure — were recorded intermittently and contained data dropouts. Therefore, the ground motion data were not digitized.

Digitization start and end times were selected for each test, and digitization requests were transmitted to the Sandia offices at Mercury, Nevada, along with duplicates of the original magnetic tapes. Sandia digitized the data at 200 samples/sec and transmitted the resulting tapes of digitized data to URS/Blume's offices in San Francisco. URS/Blume inspected these raw digitized data and created a final set of magnetic tapes containing the calibrated data in digitized form.

A small number of the digitized data were unusable because of difficulties during field testing and recording.

- The force transducer signal in dwell test M-1-L-OE was distorted by clipping and unwanted spikes. A review of the paper playback records from the original tape showed that the distortion occurred at the time of the field recording. This signal could not be restored through filtering procedures and had to be discarded.
- The signals from the fourth-mode dwell tests in Test Series OE indicated unstable test conditions. The instabilities were characterized by large changes in the structural motions with little or no change in the level of the input force. A closer inspection of the waveforms gave the impression that the structure was being excited in two different modes. Since the roof was very near to a node of the fourth mode, one might expect difficulties in exciting the fourth mode with the vibration generator located on the roof. Thus, the data from dwell tests M-4-T-OE and M-4-L-OE were not suitable for analysis.

Some data, but an almost insignificant number, were corrupted during the process of creating the digitized tapes. The signals for the second-floor velocity on the digitized tapes for dwell tests M-1-T-OE, M-2-T-OE, M-3-T-03, and M-2-L-QE were found to be incorrect in comparison with the original tapes. The digitized signals did not match the analog signals in either amplitude or waveform. This suggested that the error was not simply an incorrect value for the calibration factor or superimposed noise. This error could have originated in the process of either duplicating or digitizing the tapes. It was not important to determine the source of the error or to correct it because the second-floor velocities were only essential in the determination of mode shapes. Approximate values for second-floor velocity for use in determining mode shapes for these five tests were obtained from the paper playback records.

Data Sampling for Analysis

Short segments of the time histories in each dwell test were selected for the purpose of analyzing the digitized data. Samples were selected by inspecting the paper playback records and establishing sample start times

where the signals had already been fairly stable for about 1 sec and remained stable for about 10 sec more. Samples were numbered sequentially in each test. Start times for samples in the nondestructive tests are shown in Table 8, and sample start times for the destructive test and postdestructive tests are shown in Table 9.

The programs used in data analysis required that the number of data points in a sample be 2 to some integral power. In addition, sample lengths needed to be at least 5 sec in order to include several cycles of motion. Therefore, signal samples consisted of 1,024 digitized data points, thus providing sample lengths of 5.115 sec.

Response Data Analysis Using the RAP Program

The computer program RAP was used to analyze the 1974 response data to provide structural response characteristics, i.e., mode shapes, modal frequencies, and modal damping ratios.[17] For consistency in comparing results from the 1974 tests of the original structure with the results from the 1979 tests of the epoxy-repaired structure, it was decided to conduct the current analysis using RAP.

RAP is based on a curve-fitting method in the time domain and was originally developed by Ragget.[13] The program can be used to obtain the linear dynamic response characteristics for a particular mode from an input-output pair of time histories. A modal response is first isolated and separated from the total response by a filtering scheme. This assumes that the dynamic behavior of the structure can be well approximated by the summation of a number of responses of a viscously damped, linear, single-degree-of-freedom oscillator. The response of a theoretical single-degree-of-freedom oscillator is generated and fitted in a least-squares sense to the isolated modal response. The viscous damping ratio and the natural frequency of the best-fit oscillator are assumed to represent the response characteristics of the isolated mode. A mode shape can be obtained by using the root-mean-square (RMS) amplitudes of the best-fit responses at the various floor levels.

TABLE 8

START TIMES FOR SAMPLES IN NONDESTRUCTIVE TESTS

Sample	Start Time* (sec)					
	M-1-T-OE	M-2-T-OE	M-3-T-OE	M-1-L-OE	M-2-L-OE	M-3-L-OE
1	20.0	30.0	40.0	20.0	20.0	20.0
2	40.0	60.0	80.0	60.0	60.0	60.0
3	70.0	90.0	120.0	100.0	80.0	100.0
4	90.0	120.0	160.0	160.0	100.0	160.0
5	120.0	150.0	200.0	200.0	120.0	200.0
6	150.0	180.0	—	240.0	160.0	240.0
7	—	210.0	—	—	180.0	—
8	—	—	—	—	200.0	—
9	—	—	—	—	220.0	—
10	—	—	—	—	240.0	—
11	—	—	—	—	260.0	—
12	—	—	—	—	280.0	—

*Measured from the beginning of the digitized record

TABLE 9

START TIMES FOR SAMPLES IN DESTRUCTIVE AND POSTDESTRUCTIVE TESTS

Sample	Start Time* (sec)		
	M-1-L-PE	M-1-L-QE	M-2-L-QE
1	30.0	40.0	40.0
2	100.0	60.0	80.0
3	140.0	80.0	120.0
4	180.0	100.0	140.0
5	240.0	120.0	160.0
6	270.0	160.0	—
7	330.0	200.0	—
8	390.0	—	—
9	420.0	—	—
10	450.0	—	—
11	520.0	—	—
12	550.0	—	—
13	590.0	—	—
14	615.0	—	—
15	700.0	—	—
16	740.0	—	—
17	820.0	—	—
18	855.0	—	—
19	910.0	—	—
20	950.0	—	—
21	990.0	—	—
22	1,060.0	—	—
23	1,110.0	—	—
24	1,140.0	—	—
25	1,175.0	—	—
26	1,280.0	—	—
27	1,300.0	—	—
28	1,350.0	—	—
29	1,390.0	—	—
30	1,430.0	—	—
31	1,520.0	—	—
32	1,600.0	—	—
33	1,630.0	—	—

*Measured from the beginning of the digitized record

The version of RAP used in the analysis of the 1979 data was a modified and improved version of the previous program. Although no conceptual changes were made, the improvements were significant. The algorithm for differentiation of the force signal was changed from a simple two-point backward finite-difference scheme to a more accurate five-point scheme. Finite-difference algorithms for the solutions of the homogeneous differential equation subject to specific initial conditions were replaced by closed-form solutions. The finite-difference algorithm for the solution of the nonhomogeneous differential equation was replaced by an algorithm that solves the differential equation exactly in each time step, as developed by Nigam and Jennings.[23]

This new version of RAP, called NewRAP, was verified using a four-degree-of-freedom mathematical model subjected to an actual force time history recorded during the 1979 destructive dwell test. Both the stiffness and the damping of the mathematical model could be easily varied. Using an in-house version of the SAP IV program,[24] this model was subjected to the recorded forcing function, and the roof velocity was determined for a known stiffness (i.e., period) and a known damping ratio. In this manner, an input-output pair of time histories (in this case, force and velocity) were created as if they had been recorded from an actual structure with known dynamic characteristics. Using this input-output pair, NewRAP was used to identify the period and damping ratio of the mathematical mode. The accuracy of NewRAP could then be gauged by comparing these identified values of period and damping ratio with the known values for the mathematical model. By altering the stiffness of the model structure and resubjecting it to the same forcing function, vibrations on and around the resonant frequency were simulated.

The results of this verification study are summarized in Table 10. The frequency ratio, β, used in the table is defined by the expression:

$$\beta = \overline{f}/f \qquad (4.1)$$

where:

$\overline{f}$ = frequency of the forcing function

f = first modal frequency of the mathematical model

TABLE 10

SUMMARY OF RESULTS OF THE

VERIFICATION STUDY OF NewRAP

Frequency Ratio β	Properties of the Model		Properties As Identified by NewRAP			
	Period, T (sec)	Damping Ratio (%)	Period, T (sec)	Damping Ratio (%)	Percent Error in Period Estimate	Percent Error in Damping Estimate
0.79	0.4799	2.00	0.4729	1.53	-1.46	-23.5
0.90	0.5495	6.00	0.5469	6.13	-0.47	+2.2
	0.5495	10.00	0.5455	10.34	-0.73	+3.4
0.98	0.5986	2.00	0.5984	2.00	-0.03	0.0
	0.5986	6.00	0.5984	6.13	-0.03	+2.2
	0.5986	10.00	0.5965	10.16	-0.35	+1.6
1.22	0.7431	2.00	0.7304	2.19	-1.71	+9.5
	0.7431	6.00	0.7315	5.47	-1.56	-8.8
	0.7431	10.00	0.7326	8.84	-1.41	-11.6

Note: $\beta = \overline{f}/f$, where $\overline{f}$ is the frequency of the forcing function and f is the first modal frequency of the mathematical model.

The modal frequency is equal to the inverse of the modal period, T, identified in Table 10.

For driving frequencies at resonance or 10% below resonance, errors of 3.4% or less were observed in the ability of NewRAP to identify damping ratios as large as 10% of critical damping. For the same conditions, NewRAP identified the modal period with less than 1% error. However, when the driving frequency varied significantly from the resonant frequency, the accuracy of NewRAP decreased greatly. With the driving frequency at 22% above resonance, errors of about 10% were observed in the identified values of the damping ratios. When the driving frequency was 21% below resonance, an error of 23% was found in the identified damping ratio. However, it is interesting to note that, under the same conditions, the identified values of the modal periods were within 2% of the correct values. It was concluded that NewRAP very accurately identifies periods and damping ratios when the driving frequency is at or near the resonant frequency. As the driving frequency begins to differ from near-resonant conditions, the program is able to identify the period accurately, even though it may not be able to accurately identify the damping ratio.

In the actual application of NewRAP to the 1979 data, the program would read a prescribed sample from the time histories for the force and one or more floor velocities. Because some of the signals contained baseline offsets, a linear baseline correction subroutine was added to NewRAP that could be invoked at the beginning of the program if desired. Also, in order to check the filter parameters input to NewRAP, a subroutine was added to calculate and plot Fourier amplitude spectra of the samples. Once NewRAP had performed the baseline correction and created the Fourier amplitude spectra, if desired by the user, it proceeded to process the signals in the same general way RAP did. The output from the program provided estimates of the modal period and modal damping ratio corresponding to each floor velocity signal read into the program. The output also provided RMS values of the floor velocities from the best-fit time histories generated by the program. These RMS floor velocities were used to obtain mode shapes.

Response Data Analysis Using Other Means

In some instances, the periods were estimated directly from plots of the velocity time histories. From a computer-generated plot of the desired signal, the length of time corresponding to a selected number of cycles was determined. The period was calculated by dividing the time length by the number of cycles.

Mode shapes were also obtained in some instances by means other than the use of the NewRAP program. Concurrent samples of the floor velocities were digitally processed by a special program to obtain RMS values. (If necessary, the samples were first baseline corrected.) Mode shapes were then evaluated using these RMS values of the floor velocities and normalizing the roof velocity to unity.

5. RESULTS AND DISCUSSION OF DATA ANALYSIS

Observed Damage

The test structure was visually inspected before and after each test series. Although no damage was noted after the nondestructive tests, substantial damage occurred during the destructive test. The type and extent of the damage due to the destructive testing was similar to what might be expected from a major destructive earthquake. The pattern of damage sustained by the epoxy-repaired structure was similar to that sustained by the original structure.

The cracking at the beam-column connections appeared to be much less severe in the epoxy-repaired structure than in the original structure. Figure 10 shows the damage from the 1974 test at the northeast corner of the third floor, and Figure 11 shows the damage from the 1979 test at the same location. Figures 12 and 13 show the southeast corner of the third floor after the two tests. The damage evident in the last two figures was largely due to a construction error: a longitudinal reinforcing bar at the bottom of the beam was placed outside the confined region of the reinforcing steel in the column.

Nonsymmetrical damage occurred in both the original and epoxy-repaired structures, indicating torsional vibrations during the destructive tests. Evidence of this was cited in the report on the 1974 tests[17] and remained the same in the 1979 tests, although the damage was less.

In general, the epoxy-repaired structure was less severely damaged than the original structure. The cracking in the epoxy-repaired structure was more widely dispersed than in the original structure, with less concentrated damage at joints. This suggests that the epoxy procedure may have created better joints, probably through improved bonding between the reinforcing bars and the concrete.

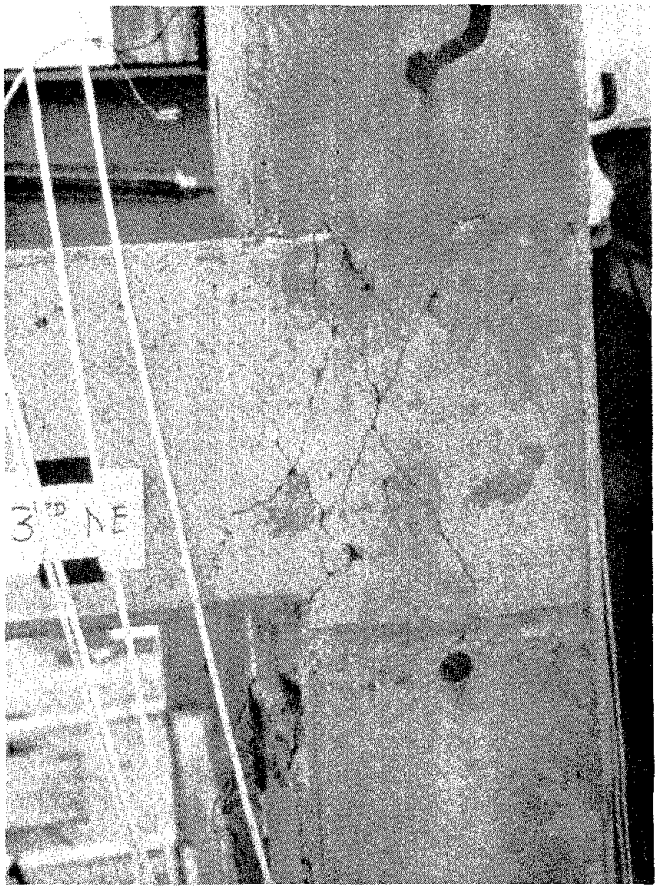

FIGURE 10 DAMAGE FROM THE 1974 TEST AT THE NORTHEAST CORNER OF THE THIRD FLOOR OF THE ORIGINAL STRUCTURE

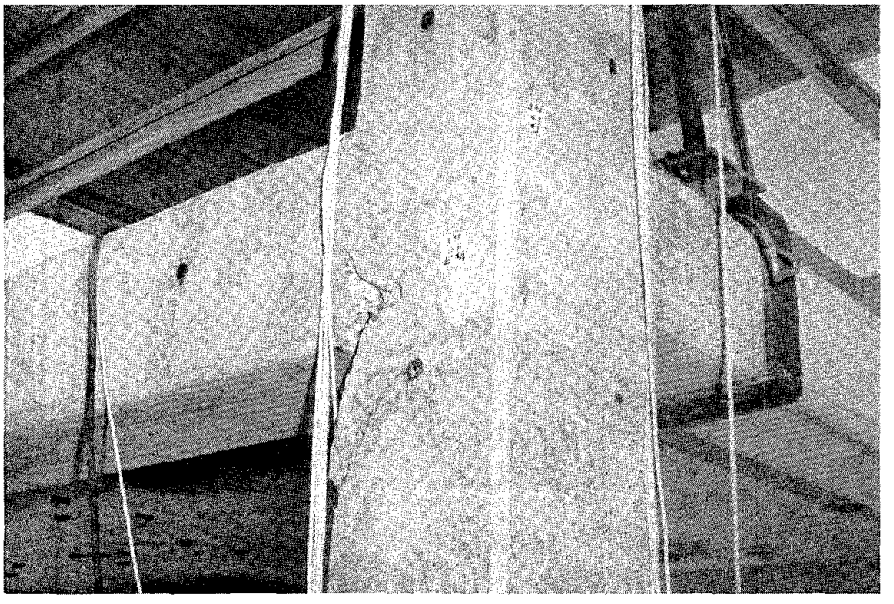

FIGURE 11 DAMAGE FROM THE 1979 TEST AT THE NORTHEAST CORNER OF THE THIRD FLOOR OF THE EPOXY-REPAIRED STRUCTURE

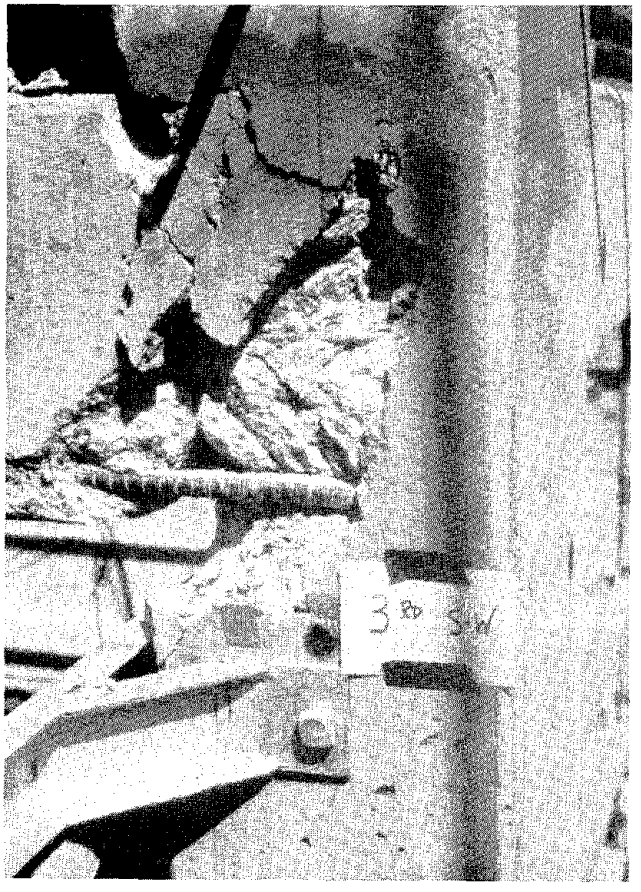

FIGURE 12 DAMAGE FROM THE 1974 TEST AT THE SOUTHWEST CORNER OF THE THIRD FLOOR OF THE ORIGINAL STRUCTURE

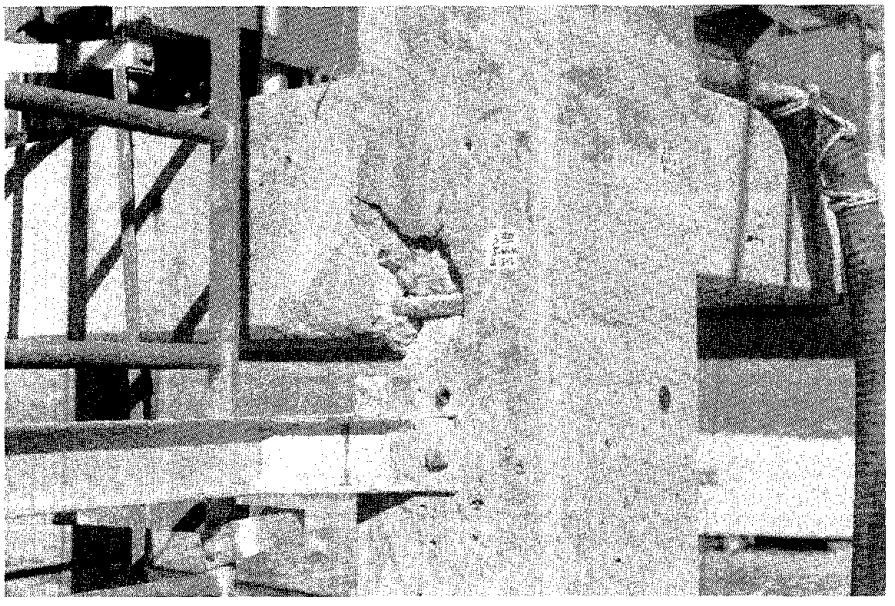

FIGURE 13 DAMAGE FROM THE 1979 TEST AT THE SOUTHWEST CORNER OF THE THIRD FLOOR OF THE EPOXY-REPAIRED STRUCTURE

Structural Damping

Efforts to determine the modal damping ratios in the epoxy-repaired structure were not successful. An analysis of the dwell test data yielded conflicting and enigmatic results. These findings are presented and discussed below.

Driving Force. Although modal periods and mode shapes can be determined from only the floor velocities in the dwell test, modal damping values require knowledge of the input driving force as well. In the 1974 tests, the signal from the force transducer was the only available measure of the driving force. Since some of the input force was lost in friction at the wheels, the amplitude of the force transducer signal was reduced by a constant value to account for wheel friction in the analysis of the 1974 test data. This procedure was logically based on the theory that the magnitude of the actual driving force will be smaller than the input force and that this difference in magnitude will become negligible as the input force is increased to levels that cause major damage. However, the friction force will also create a phase shift between the input force and the actual driving force, a fact that was not included in the corrections to the input force for the 1974 data.

In the 1979 tests of the epoxy-repaired structure, the signal from the accelerometer on the reaction mass was recorded simultaneously with the floor velocities. The accelerometer signal should represent the actual driving force and not require correction for wheel friction. The force transducer signal should be similar in amplitude and waveform to the accelerometer signal multiplied by the reaction mass, except possibly in the low-amplitude range where friction is significant. However, a comparison showed great discrepancies and failed to indicate which signal was the better measure of the driving force.

Figure 14 shows the relationship between the RMS amplitudes of the two measures of the driving force — the reaction mass times the accelerometer signal (ma) versus the force transducer signal (F) — over a range of force levels. The behavior in the low-amplitude transverse vibration tests (M-1-T-OE and M-2-T-OE) was as expected: ma was smaller than F for low values

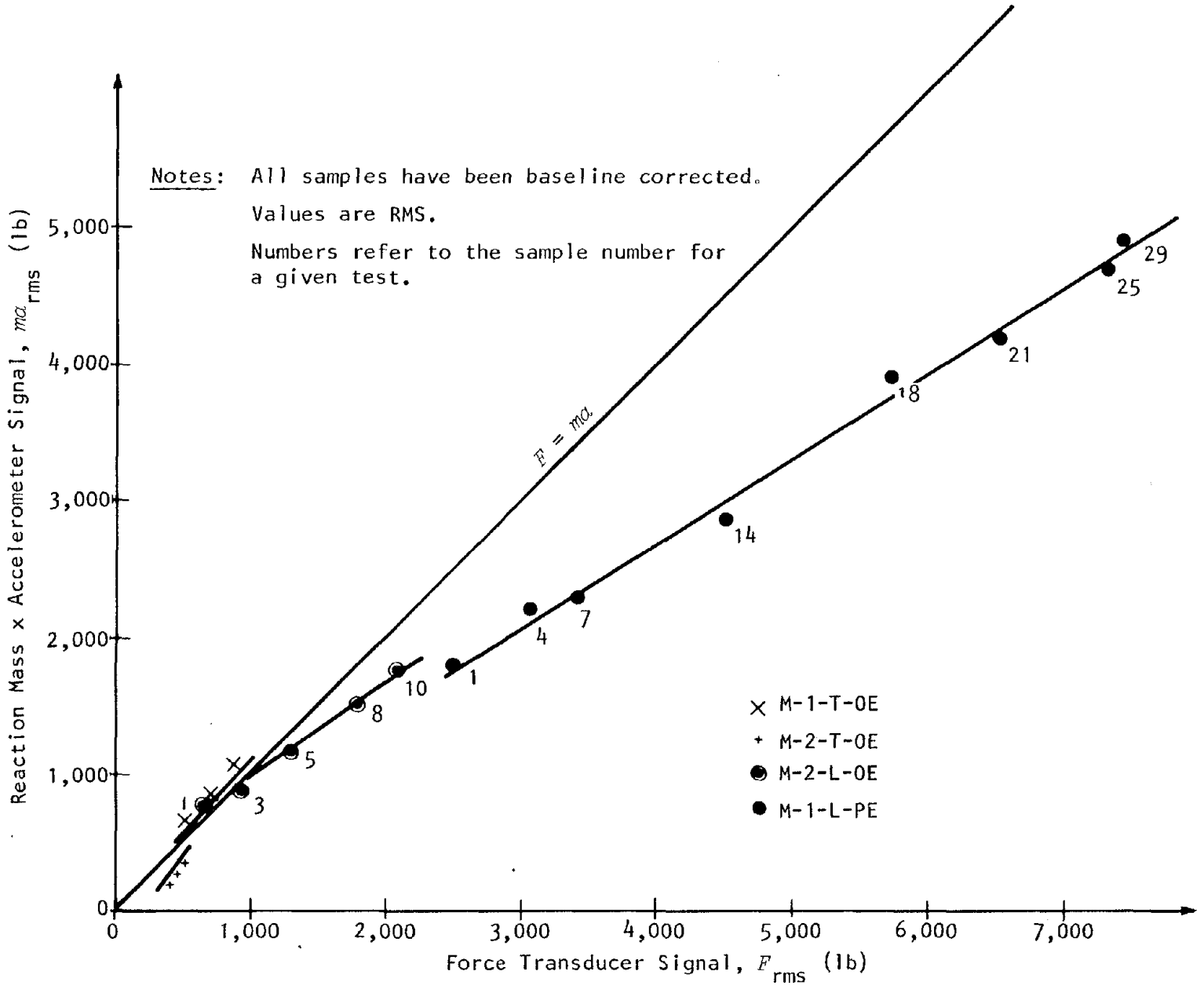

FIGURE 14 RELATIONSHIP BETWEEN TWO MEASURES OF THE DRIVING FORCE

where friction was most significant, and $m\alpha$ approached F as the force level increased. But this relationship did not hold in the longitudinal tests. In both the low-amplitude test (M-2-L-OE) and the high-amplitude destructive test (M-1-L-PE), the relationship between $m\alpha$ and F was linear, but $m\alpha$ was less than F.

If the difference between the amplitudes of $m\alpha$ and F is credited to the frictional force, this plot suggests that the frictional force did not remain constant but rather increased as input force increased. There was nothing to suggest that frictional losses could increase in this way or become so large. Since the difference cannot be ascribed to frictional losses, this behavior may suggest a possible calibration error. However, the presence of a calibration error could not be verified. Laboratory calibration data for the force transducer and notes on field calibration for both the accelerometer and force transducer were reviewed, but no errors or discrepancies were discovered.

The field notes contained entries of the force levels at various times during the destructive test. These entries, which were recorded from a gauge in the instrumentation trailer, were typically smaller than the RMS values for F but larger than the values for $m\alpha$. Furthermore, field personnel regarded the values from the force gauge in the trailer as peak values, not RMS values. No matter whether the gauge was reading RMS or peak values, the gauge value did not correspond to either the F or $m\alpha$ values. Thus, the field notes did not provide a clear indication of which signal — the force transducer or the accelerometer — would provide the better measure of the driving force.

Damping Values. Damping values were obtained for several modes using data from nondestructive and destructive dwell tests. Both the force transducer and the accelerometer signals were used to represent the driving force in the NewRAP program. It was hoped that the NewRAP results might indicate which signal would better represent the driving force; however, no clear pattern emerged.

Figure 15 shows the values of damping ratios obtained from the 1979 destructive test using both the force transducer (dots) and the accelerometer

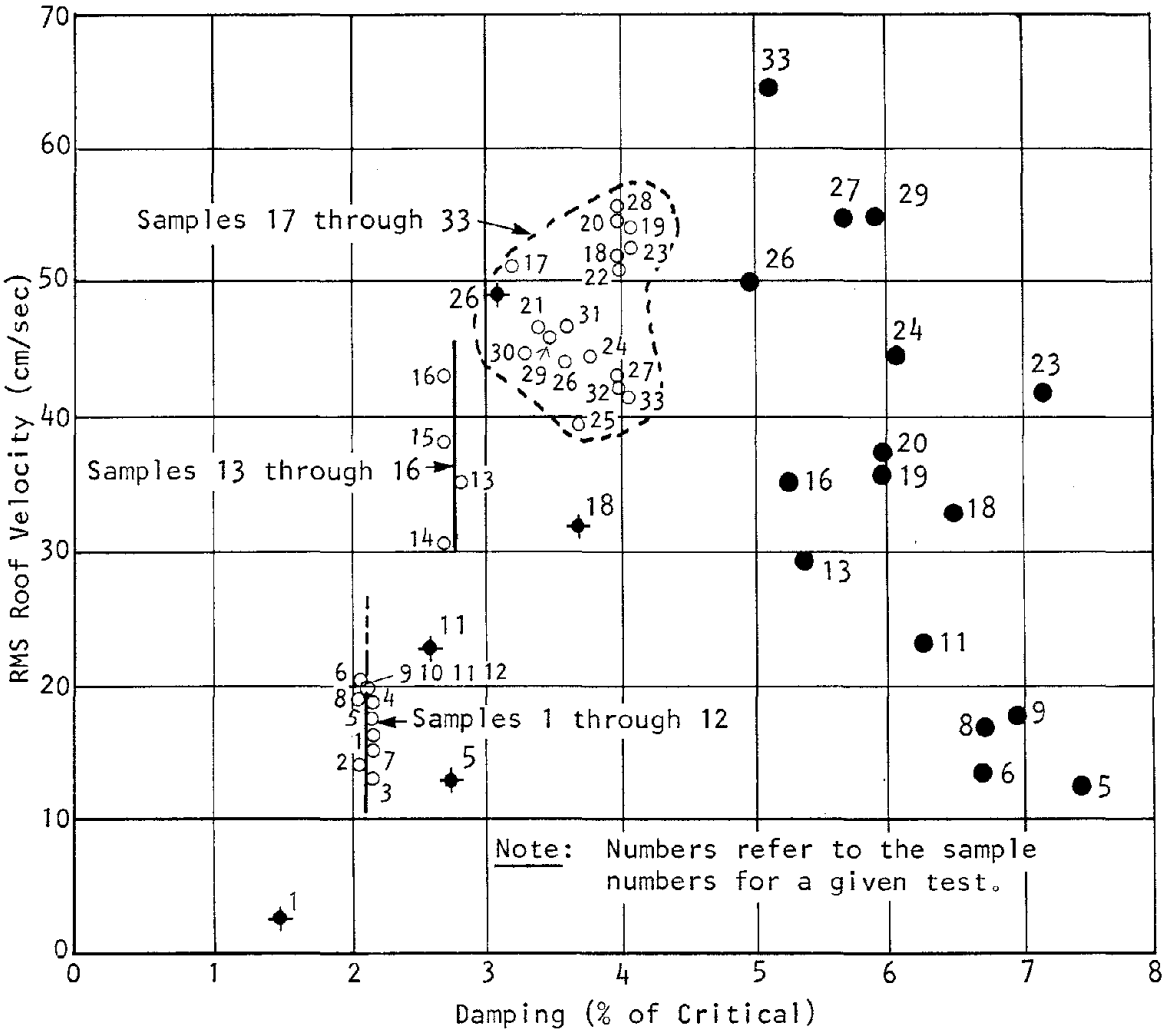

FIGURE 15 VELOCITY VERSUS DAMPING FOR DESTRUCTIVE TEST, LONGITUDINAL DIRECTION

(dots with cross hairs) superimposed on the 1974 test results. The force transducer signal was not reduced to account for the frictional force; however, this was not a significant omission because the frictional force was very small compared with the total force.

In general, the 1979 values obtained from the force transducer seem too large in comparison with the 1974 values. It is known that movement over a dispersed network of cracks will dissipate more energy than the same movement over a single crack. Since the epoxy-repaired structure appeared to have a greater number of active cracks, a greater amount of structural damping should be expected. This could explain damping values of 6% at high roof velocities in the 1979 destructive test in comparison with values of 3% to 4% in the 1974 destructive test. However, damping values of 7% at low roof velocities in the 1979 test cannot be explained.

The damping values obtained for the destructive test using the accelerometer signal seem more reasonable. This suggested that the force transducer was unreliable and that the accelerometer signal should be used. Unfortunately, this conclusion was not supported by results from other tests.

In the low-amplitude, second-mode, longitudinal test (M-2-L-OE), the damping values obtained using the accelerometer signal were only somewhat smaller than those obtained using the force transducer (see Figure 16). The exception to this observation occurred at very low amplitudes (RMS roof velocities on the order of 2 cm/sec), where damping values obtained using acceleration were a great deal smaller. The negative slope in the general trend for damping values with increasing roof velocity in this low-amplitude test is not logical and raises doubts about the validity of the data from this test.

In the low-amplitude, first-mode, transverse test (M-1-T-OE), damping values of 5.5% to 6.8% were obtained using the reaction mass acceleration, whereas use of the force transducer signal yielded values of 10.5% to

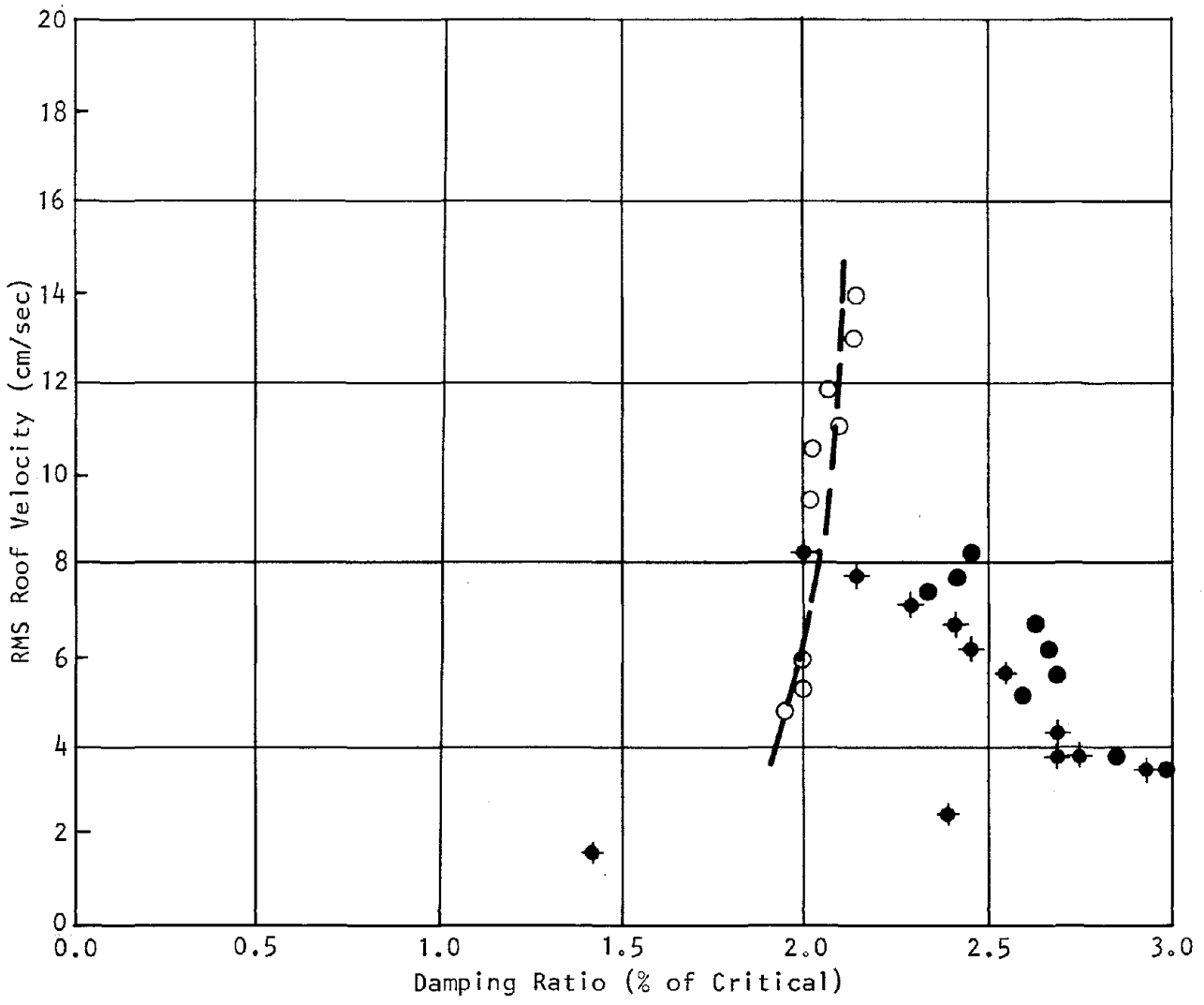

FIGURE 16 VELOCITY VERSUS DAMPING FOR THE SECOND-MODE LONGITUDINAL NONDESTRUCTIVE TEST

12.7%. These values seem unrealistically high in comparison with values of 1.4% to 2.0% obtained from the equivalent 1974 test.

In the second-mode transverse test (M-2-T-OE), damping values of 2.3% to 2.5% were obtained using the force transducer, whereas the accelerometer signal yielded values ranging from 1.9% to 5.1%. In this test, the force transducer appeared to provide more reasonable values of damping in comparison with values of 1.8% to 2.3% obtained from the equivalent 1974 test.

Thus, the damping values themselves did not indicate a logical choice for the correct representation of the driving force.

Instrumentation Phase Characteristics. Phase shifts could have existed between the L-7 velocity meters and the force transducer and the reaction-mass accelerometer. If this were so, the shifts could have affected the NewRAP analysis. The phase characteristics of the force transducer were not known and could not be determined because the instrumentation was disassembled after the 1979 tests and used in other projects at Sandia in Albuquerque. However, the phase characteristics of the L-7 transducer were evaluated with respect to a Sunstrand accelerometer. The results suggested the existence of a linear phase shift with an average time delay of approximately 0.018 sec relative to the Sunstrand accelerometer. On the basis of this finding, the accelerometer signal for the M-2-T-OE test was delayed by that amount in NewRAP runs to account for the time delay in the velocity due to the L-7 velocity meter. However, the results were not an improvement over previous calculations and failed to identify linear phase shift as the problem.

Conclusion Regarding Structural Damping. These efforts to determine the proper representation for the input driving force produced contradictory and confusing results. Since these contradictions seemed to be unresolvable, the effort to obtain structural damping was abandoned.

Mode Shapes

The mode shapes for the epoxy-repaired structure are plotted in Figures 17 through 20. The values for the mode shapes were derived using RMS values of the floor velocities by procedures described in Chapter 4. Unless otherwise noted, the values represent averages of all samples considered in a particular dwell test.

The mode shapes for the original structure are superimposed on these plots for comparative purposes. These shapes were reproduced from the report on the 1974 tests[17] unless otherwise noted below.

The first three mode shapes in the transverse and longitudinal directions are plotted in Figures 17 and 18, respectively. These plots were derived from data from the nondestructive dwell tests and, therefore, essentially represent elastic deformations. A comparison of the plots for the epoxy-repaired structure with those for the original structure shows that the behavior of the structure in the two states was very similar.

The fundamental mode shape for the epoxy-repaired structure during the destructive test is illustrated in Figure 19 by two plots. The first plot, labeled "no structural damage," depicts the mode shape early in the test before damage had occurred. It corresponds to Sample 9 and is representative of the mode shapes for other samples during the early portions of the test. The second plot shows the mode shape later in the test after major damage had occurred. It was obtained for Sample 27 and is representative of mode shapes for samples at the end of the test. The superimposed plots of the mode shapes from the 1974 test data for the original structure indicate very close agreement between the two structures during destructive testing. (The plot of the mode shape for the original structure at major damage is not the same as the one presented in Reference 17. The digitized data for the destructive test of the original structure were reanalyzed using the same procedures used on the 1979 data. The resulting mode shape for major damage is plotted in Figure 19.)

The first two mode shapes for the longitudinal direction obtained from the postdestructive test are plotted in Figure 20. A comparison with the same

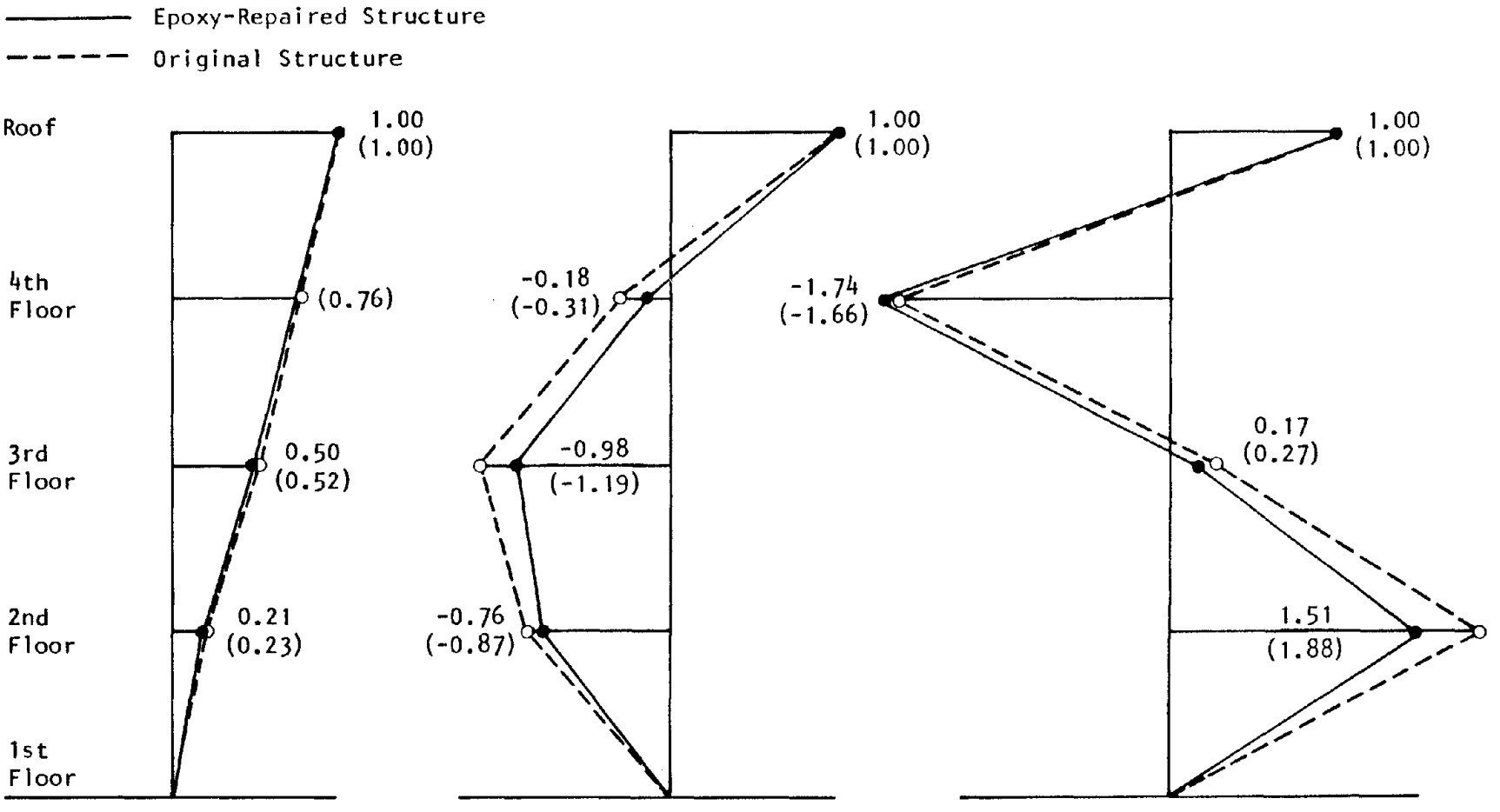

T_1 = 0.54-0.55 sec (0.45-0.51)

a. First Mode

T_2 = 0.14-0.15 sec (0.14-0.15)

b. Second Mode

T_3 = 0.074-0.079 sec (0.073-0.079)

c. Third Mode

Note: Values shown in parentheses are for the original structure.

FIGURE 17 NORMALIZED MODE SHAPES FOR THE NONDESTRUCTIVE TEST, TRANSVERSE DIRECTION

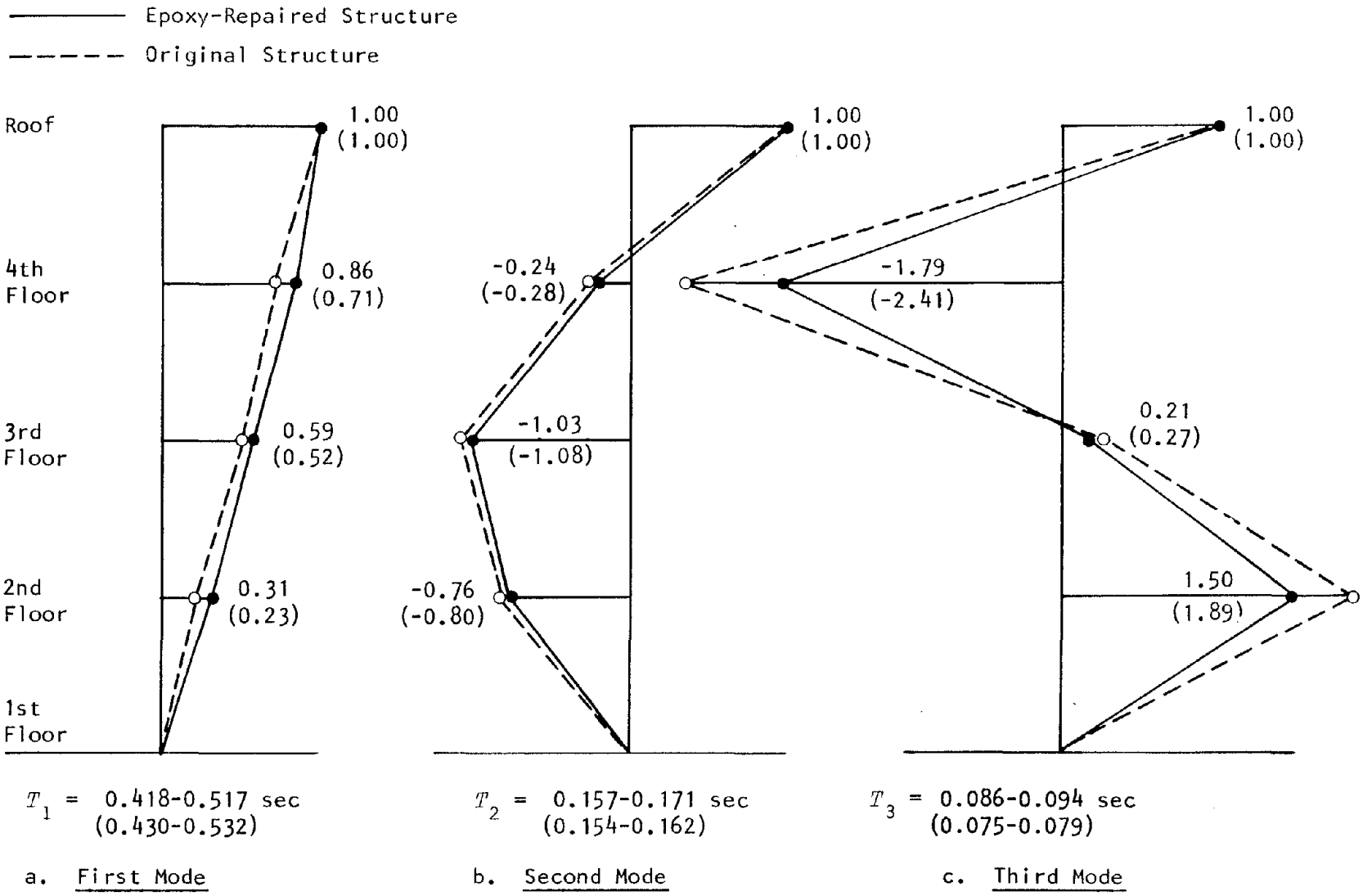

T_1 = 0.418-0.517 sec (0.430-0.532)

a. First Mode

T_2 = 0.157-0.171 sec (0.154-0.162)

b. Second Mode

T_3 = 0.086-0.094 sec (0.075-0.079)

c. Third Mode

Note: Values shown in parentheses are for the original structure.

FIGURE 18 NORMALIZED MODE SHAPES FOR THE NONDESTRUCTIVE TEST, LONGITUDINAL DIRECTION

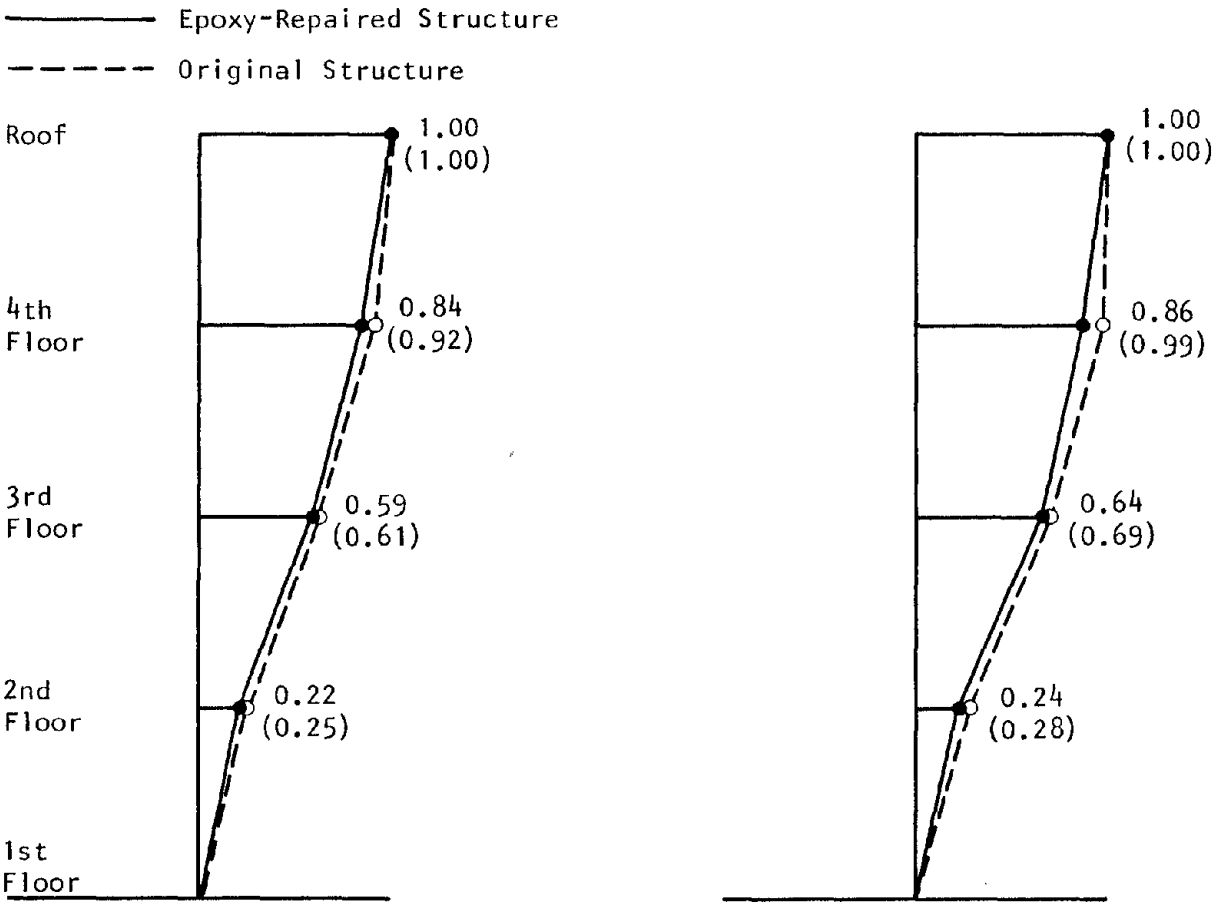

a. No Structural Damage

b. Major Structural Damage

Note: Values shown in parentheses are for the original structure.

FIGURE 19 NORMALIZED FIRST-MODE SHAPES FOR DESTRUCTIVE TEST, NO DAMAGE AND MAJOR DAMAGE, LONGITUDINAL DIRECTION

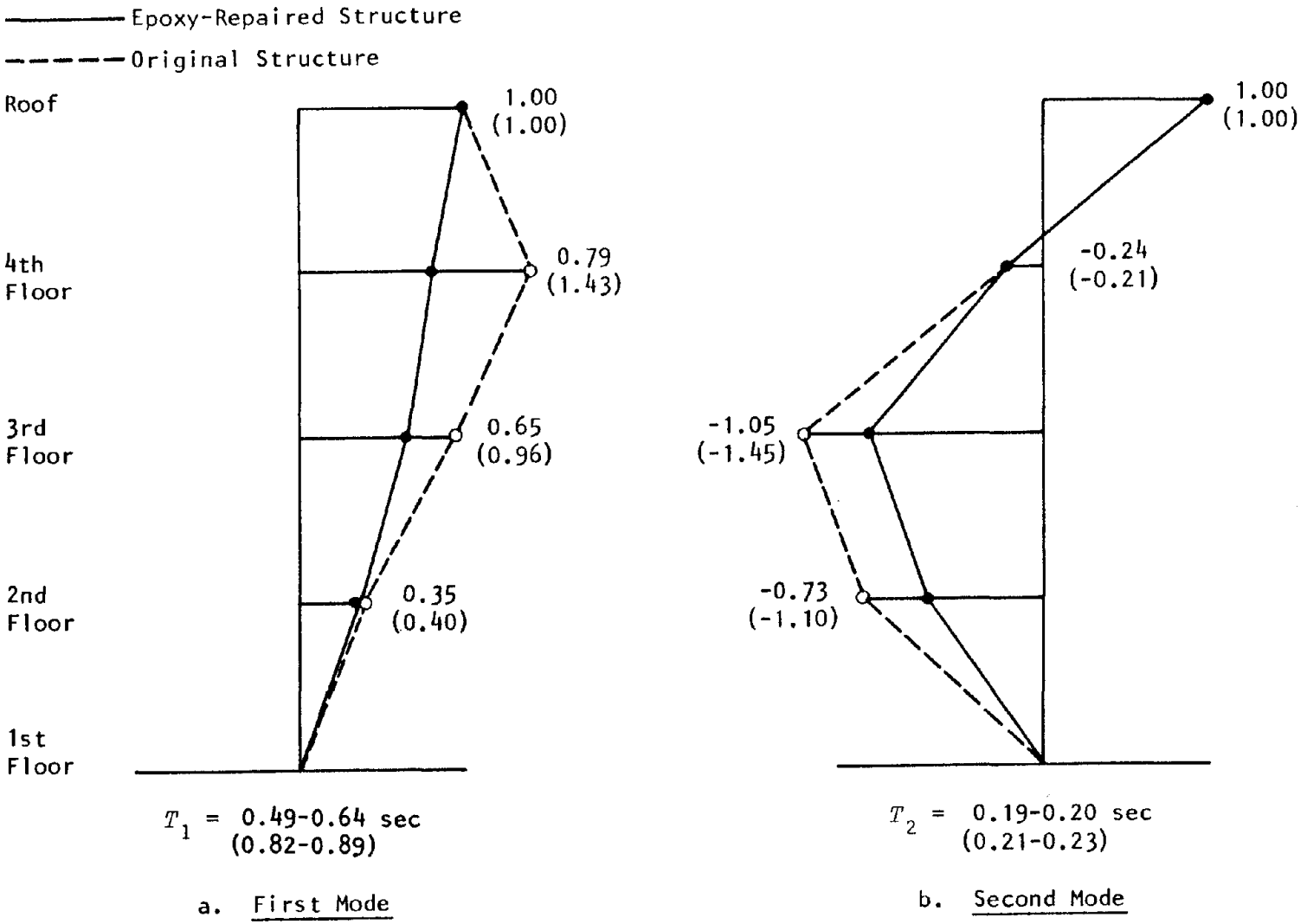

Note: Values shown in parentheses are for the original structure.

FIGURE 20 NORMALIZED MODE SHAPES FOR THE POSTDESTRUCTIVE TEST, LONGITUDINAL DIRECTION

mode shapes before destructive testing (see Figures 18a and 18b) reveals little change in the mode shapes of the epoxy-repaired structure at low-amplitude vibrations although the structure had sustained major damage. However, a comparison with the superimposed mode shapes from the postdestructive testing of the original structure indicates significant dissimilarities between the epoxy-repaired and the original structures following major damage.

Modal Periods

The periods of the first three transverse modes for the epoxy-repaired structure are compared with the corresponding periods for the original structure in Figure 21. The data were obtained from the nondestructive tests and represent low-amplitude vibrations. The plots show that the transverse stiffness of the epoxy-repaired structure was less than that of the original structure in the first mode but essentially the same in the second and third modes.

The periods of the first three longitudinal modes are compared in Figure 22, also using data from the nondestructive tests. These plots show that the epoxy-repaired structure was less stiff than the original structure in all three of these longitudinal modes, particularly in the first mode.

The changes in the fundamental longitudinal period during the destructive test are illustrated in Figure 23. At low amplitudes of motion at the start of the test, the period of the epoxy-repaired structure was greater than that of the original structure, indicating a less stiff structure. As the driving force was increased (represented in this plot by an increase in roof velocity), the period of the epoxy-repaired structure increased while the period of the original structure remained constant. However, as the driving force imparted roof velocities exceeding about 30 cm/sec, the period of the original structure began to lengthen at a much faster rate than that of the epoxy-repaired structure. By the end of the destructive tests, the period of the epoxy-repaired structure was not as great as the period of the original structure. This means that the stiffness of the epoxy-repaired structure did not degrade as much as that of the original structure, a conclusion supported by the damage observation.

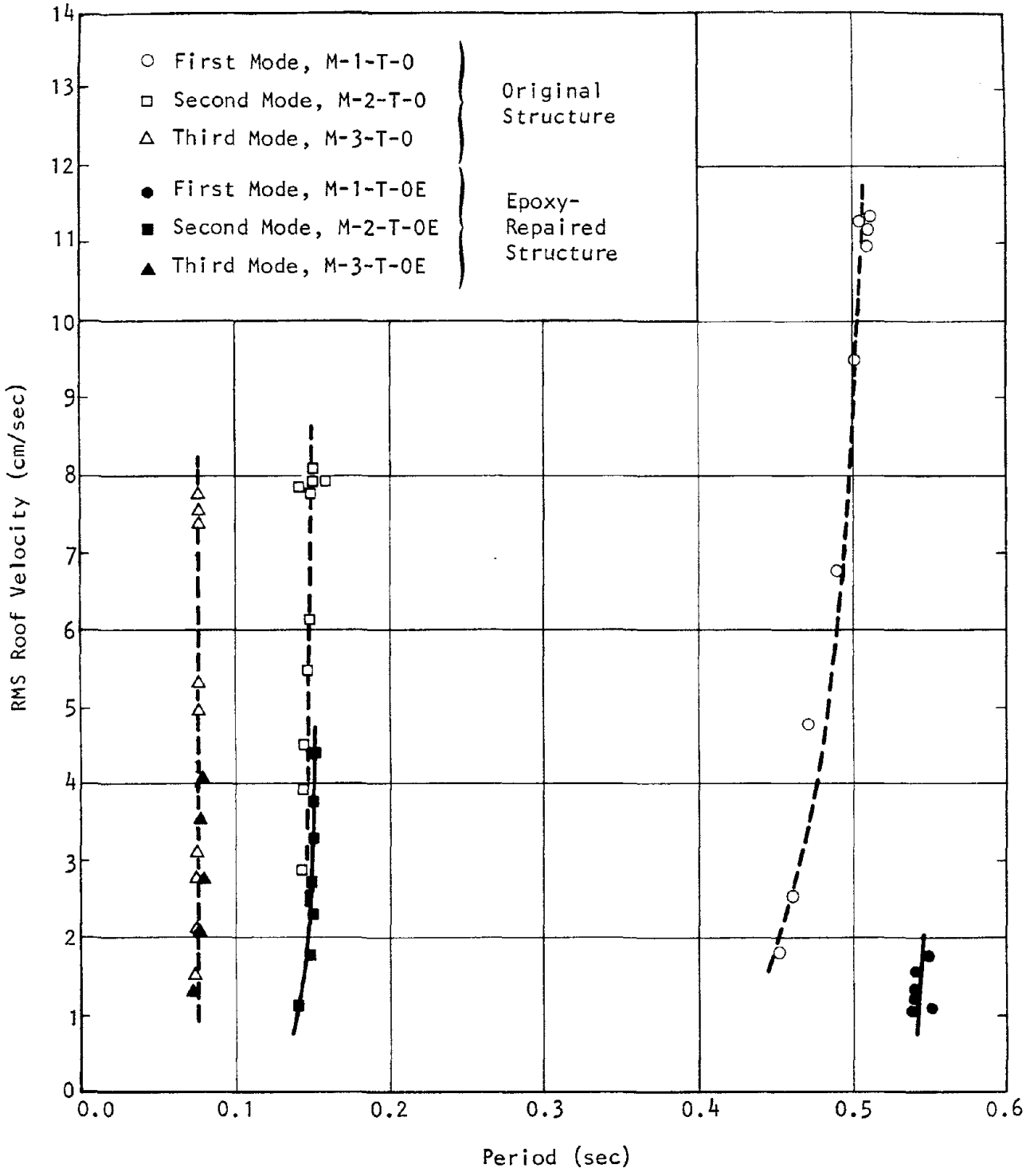

FIGURE 21 VELOCITY VERSUS PERIOD FOR THE NONDESTRUCTIVE TEST, TRANSVERSE DIRECTION

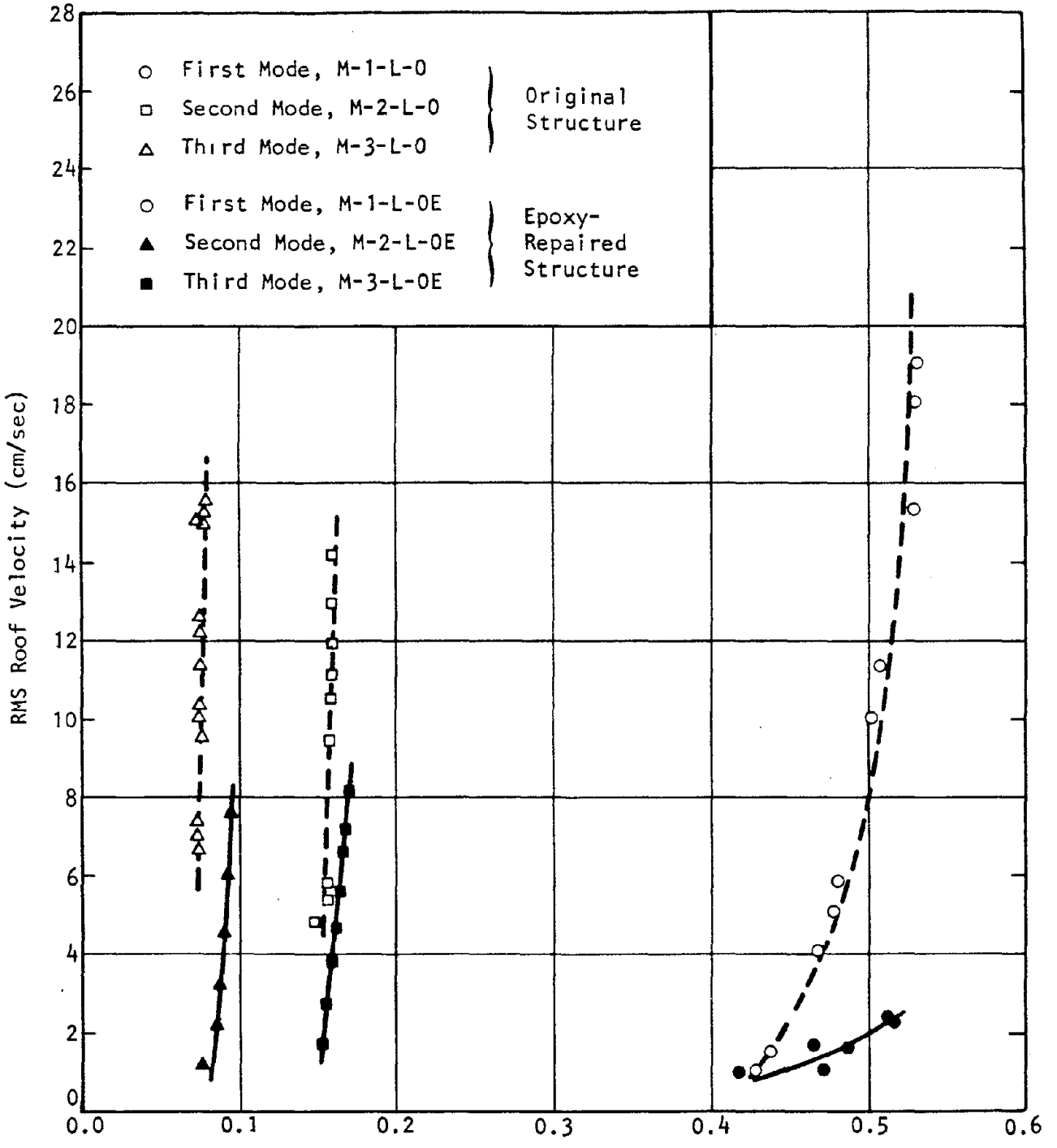

FIGURE 22 VELOCITY VERSUS PERIOD FOR THE NONDESTRUCTIVE TEST, LONGITUDINAL DIRECTION

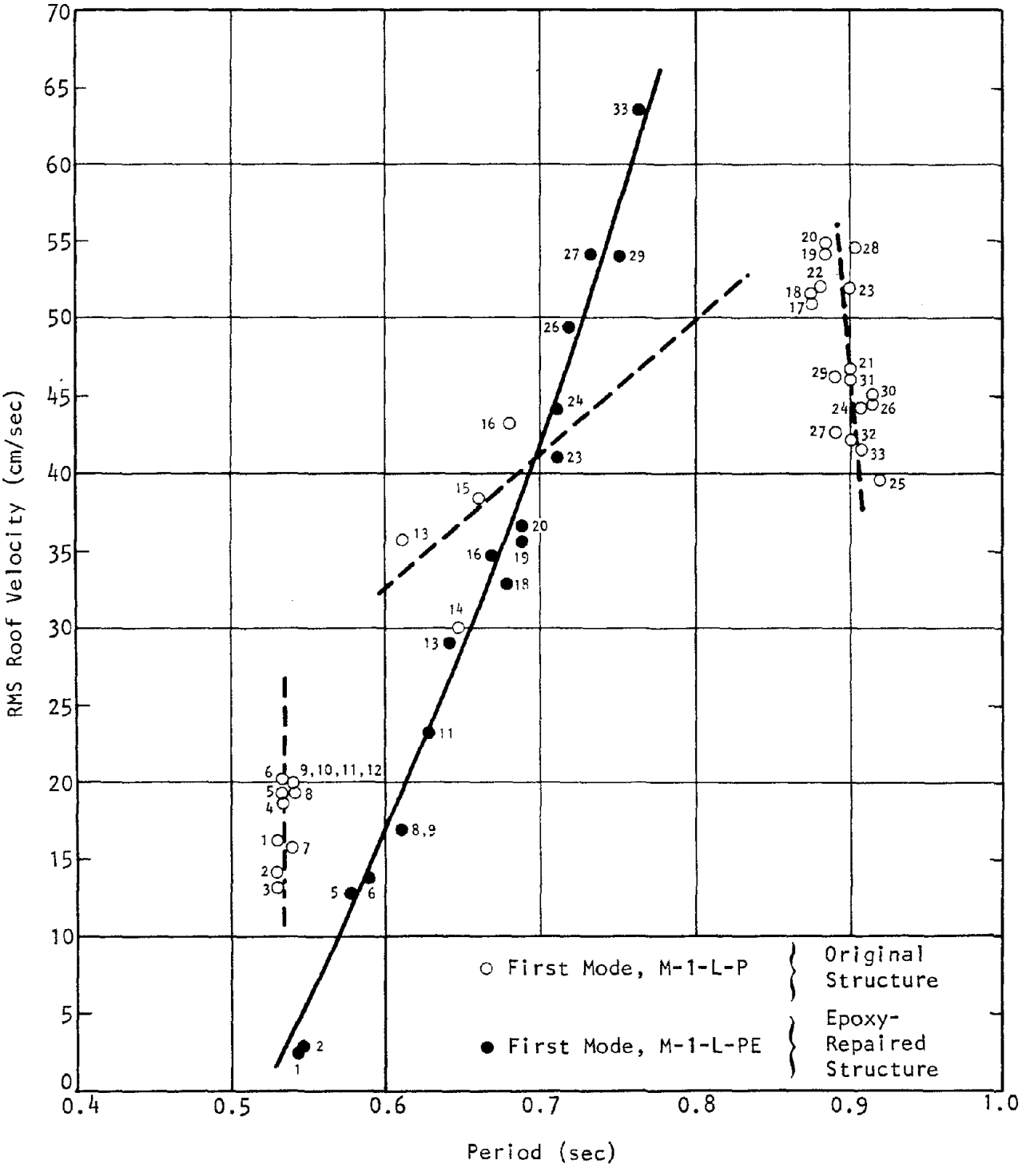

Note: The data points are numbered in the order of their occurrence, and the numbers correspond to the sample numbers.

FIGURE 23 VELOCITY VERSUS PERIOD FOR THE DESTRUCTIVE TEST, LONGITUDINAL DIRECTION

The periods of the first two longitudinal modes at low-amplitude motion following the destructive test are illustrated in Figure 24. The period of the second mode for the epoxy-repaired structure was in close agreement with that of the original structure. The period of the first mode was lower in the epoxy-repaired structure; however, it is difficult to compare the first-mode periods because the 1979 first-mode dwell test was conducted at a much lower force level.

Stiffness Degradation Versus Drift

The information on the fundamental longitudinal period from Figures 22 and 23 has been replotted in terms of stiffness versus roof displacement and presented in Figure 25. The stiffness of the fundamental longitudinal mode is proportional to the square of the modal frequency, which is equal to the inverse of the square of the modal period. The roof displacement is related to the roof velocity by the following expression:

$$d = \frac{vT}{2\pi} \tag{5.1}$$

where:

d = roof displacement
v = roof velocity
T = modal period

This plot provides a more direct representation than Figure 23 of the changes in the stiffness of the structure in the original and epoxy-repaired states as it was subjected to the destructive test program. The two structures had essentially the same stiffnessses at very low roof displacements; however, the stiffness of the epoxy-repaired structure fell dramatically with respect to the original structural stiffness as the roof displacement increased to about 1 cm. As the roof displacement increased further, the difference decreased. At a roof displacement of about 7 cm, the stiffness of the original structure underwent a significant degradation; the epoxy-repaired structure continued to degrade in a very gradual fashion. This is further evidence that the epoxy-repaired structure possessed better beam-column connections than the original structure.

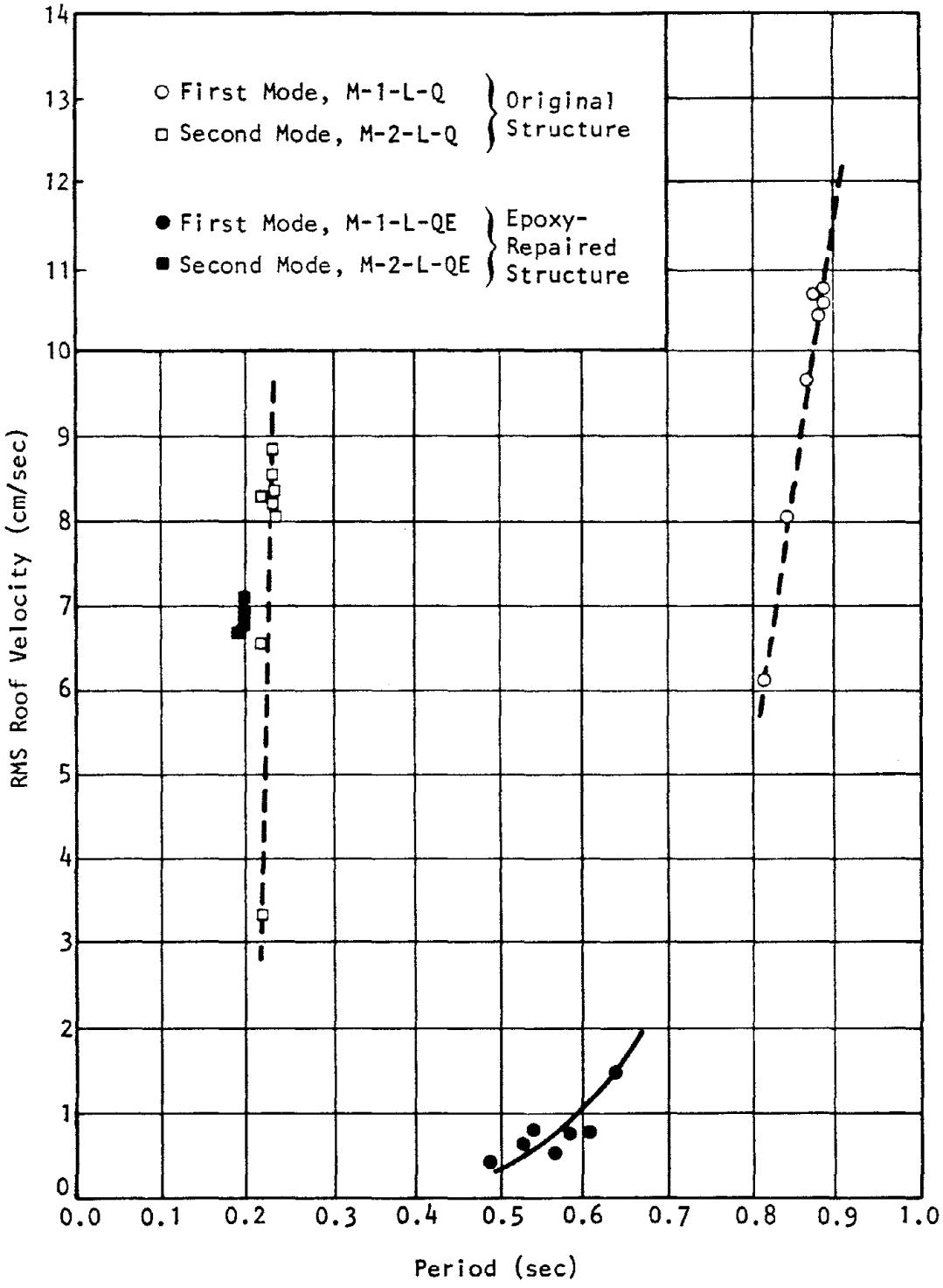

FIGURE 24 VELOCITY VERSUS PERIOD FOR THE POSTDESTRUCTIVE TEST, LONGITUDINAL DIRECTION

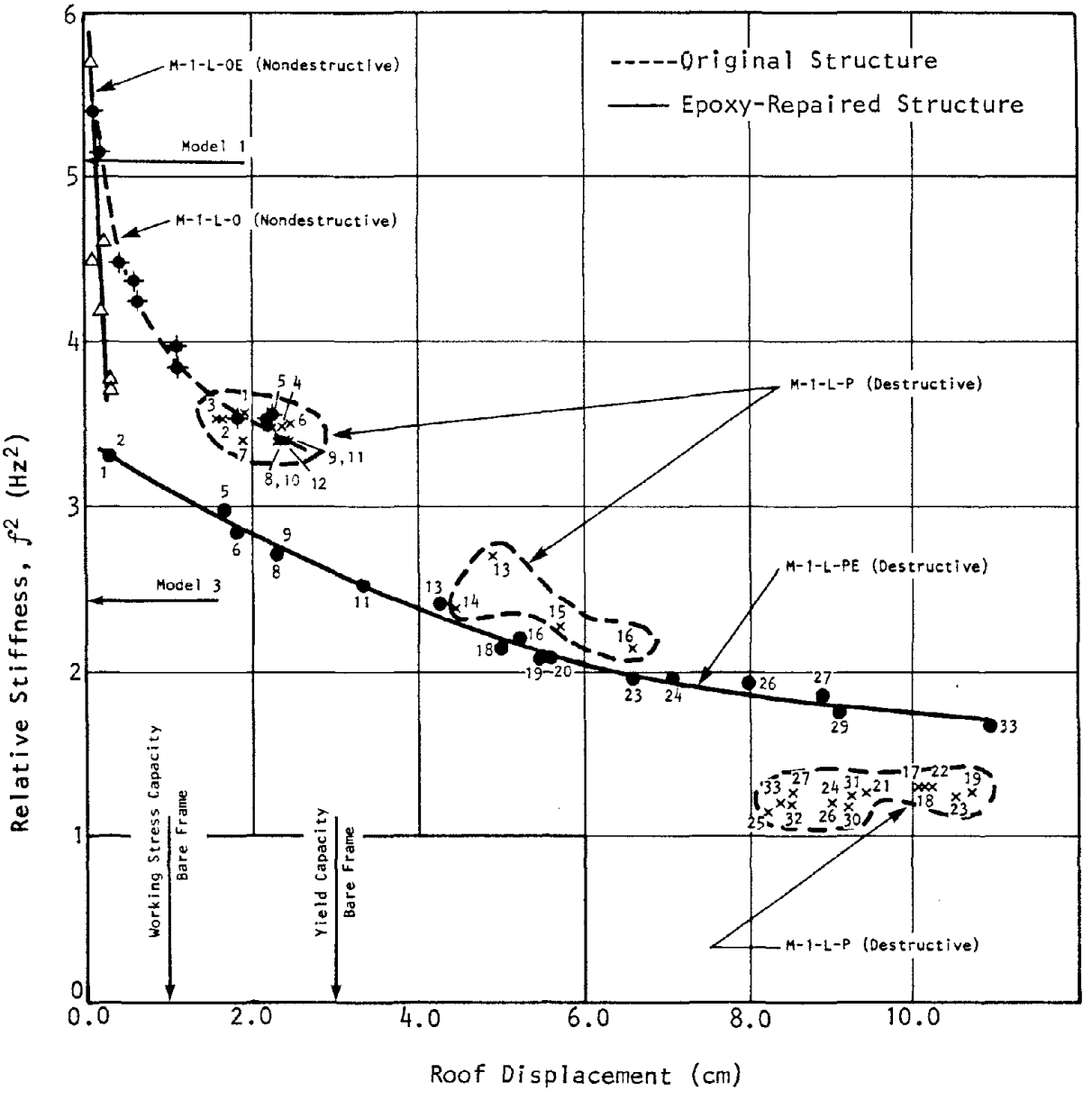

FIGURE 25 STIFFNESS VERSUS ROOF DISPLACEMENT FOR THE NONDESTRUCTIVE AND DESTRUCTIVE TESTS OF THE ORIGINAL AND EPOXY-REPAIRED STRUCTURES, FIRST MODE

References to model number and capacity in Figure 25 are discussed in Chapter 6.

Figure 26 is a replot of Figure 25 with roof displacement converted to maximum interstory drift expressed as a percentage of the story height. Maximum interstory drift percentage was determined by multiplying the roof displacement by the maximum interstory deformation from the mode shape (normalized to the roof deformation), and dividing by the story height. The 1982 *UBC*[10] limits the interstory drift to 0.5% of the story height. It is interesting to observe where this design limit occurs in Figure 26.

Base Shear

Another useful way of comparing the performance of the epoxy-repaired structure with that of the original one is to compare the base shears during the destructive tests. At any instant of time, the equilibrium of forces requires that the base shear be equal to the sum of the driving force and the inertial forces at each floor. Since the test structure was vibrating essentially in the first mode, the base shear can be defined by this expression:

$$V_0(t) = F_0(t) + \omega^2 u_4(t) \sum_{i=1}^{4} m_i \phi_{i1} \qquad (5.2)$$

where:

$V_0(t)$ = base shear during the destructive test
$F_0(t)$ = driving force
ω = fundamental circular frequency
$u_4(t)$ = roof displacement
m_i = mass of floor i
ϕ_{i1} = modal deformation of floor i for the first mode normalized to the roof

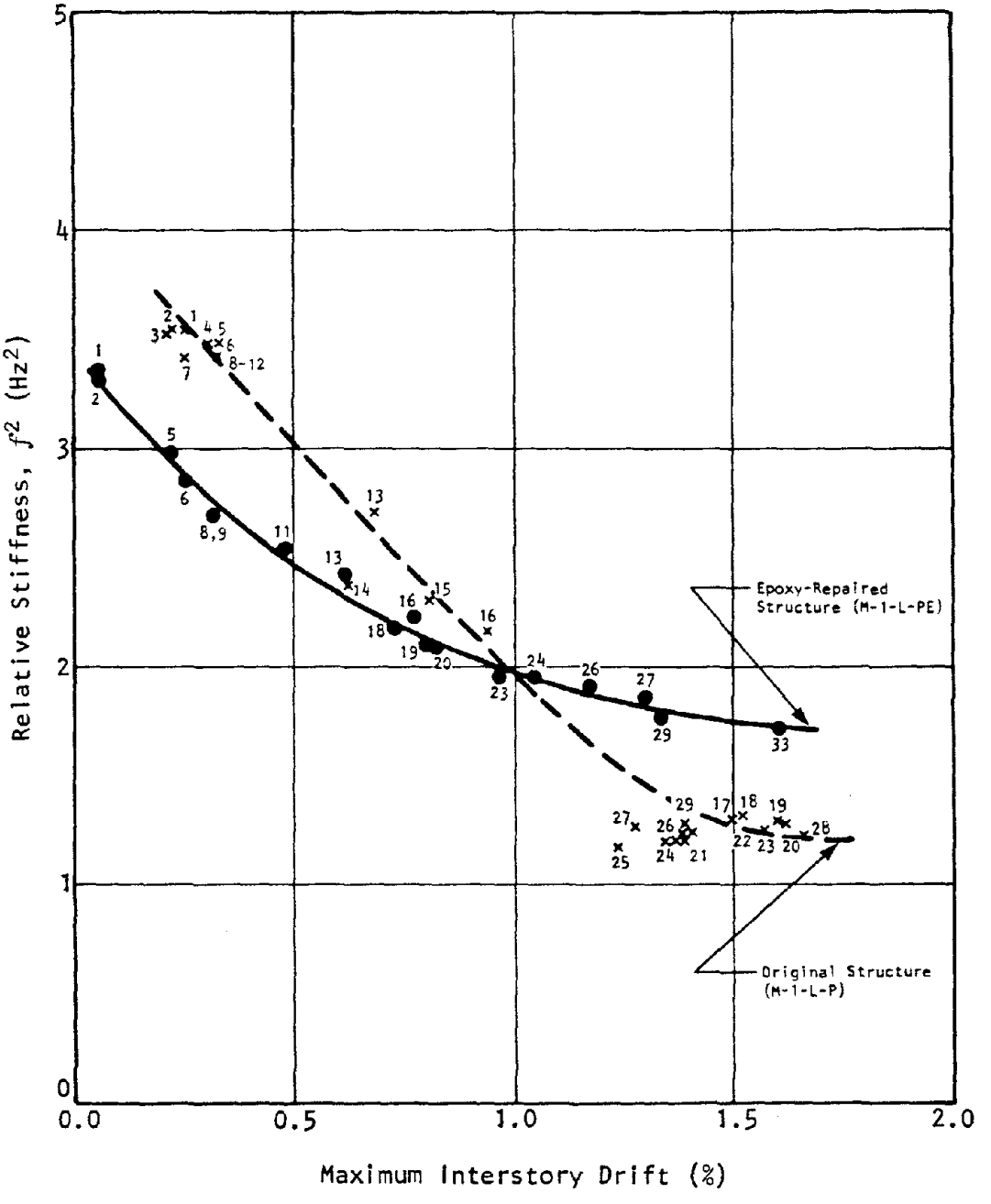

FIGURE 26 STIFFNESS VERSUS MAXIMUM INTERSTORY DRIFT FOR THE DESTRUCTIVE TESTS OF THE ORIGINAL AND EPOXY-REPAIRED STRUCTURES, FIRST MODE

The driving force and the response are essentially sinusoidal functions; therefore, Equation (5.2) can be visualized as the vector resultant of two vectors — one representing the driving force and the other the sum of the inertial forces — rotating with a fixed phase angle between them. Since the response is at resonance, the two vectors are at approximately 90°. Furthermore, assuming that the damping ratio is between 2% and 5% of critical damping, the dynamic amplification factor is large, and the vector representing the inertial forces is roughly an order of magnitude larger than the driving force vector. Consequently, the amplitude of the base shear can be approximated by the amplitude of the sum of the inertial forces at each floor, as in the following equation:

$$V_0 = \frac{\omega^2 u_4}{g} \sum_{i=1}^{4} w_i \phi_{i1} \qquad (5.3)$$

where:

V_0 = amplitude of the base shear
ω = fundamental circular frequency
u_4 = amplitude of the roof displacement
w_i = weight of floor i
ϕ_{i1} = modal deformation of floor i for the first mode normalized to the roof
g = gravitational constant, 32.2 ft/sec/sec

Data from both the 1974 and 1979 destructive tests were analyzed using Equation (5.3); the results are plotted in Figure 27. The displacement units were changed from centimeters to inches in this plot because it was felt that most United States designers would find those units more meaningful. References to yield capacity are explained and discussed in Chapter 6.

The curves from both tests seem to be identical up to a roof displacement of 2.5 in. The curves are bilinear in that range, with a well-defined change in slope at a roof displacement of about 1.0 in. It is hypothesized

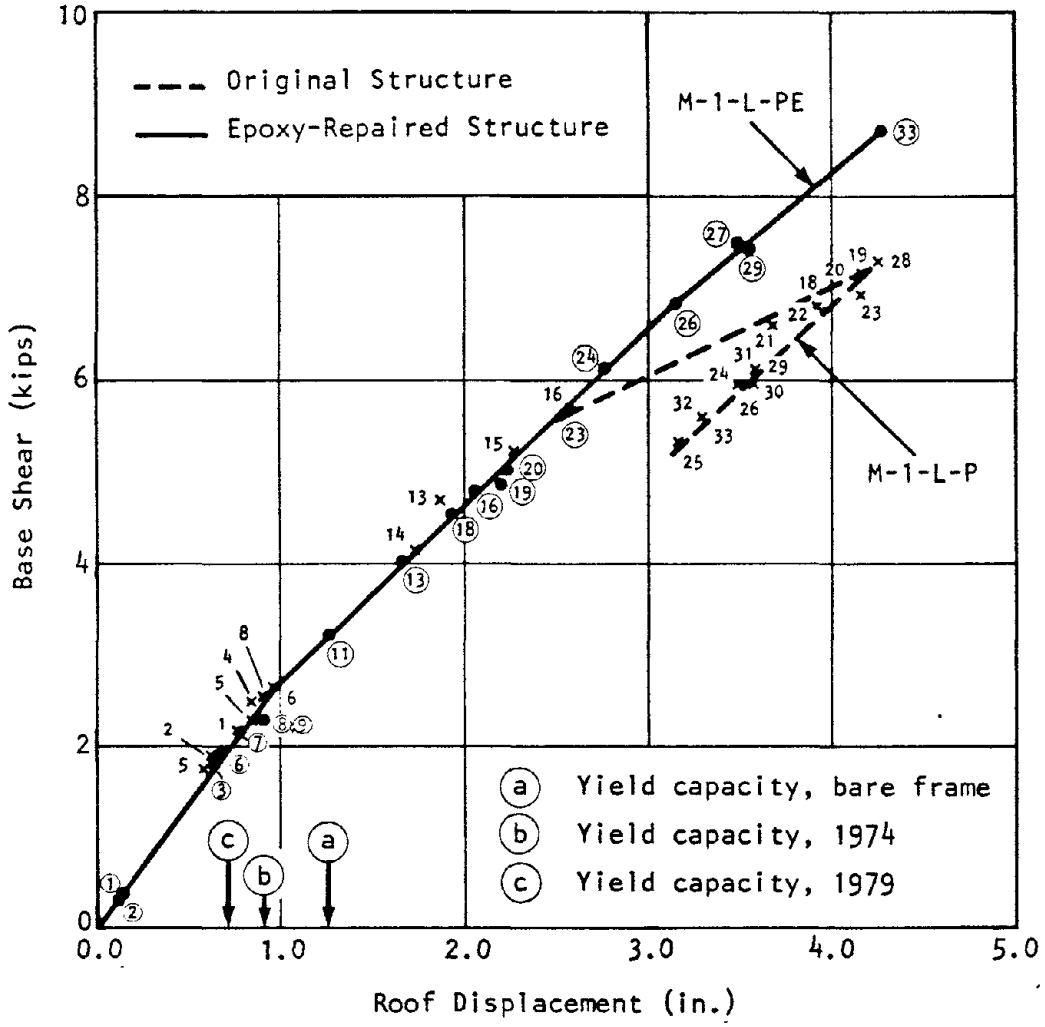

FIGURE 27 BASE SHEAR VERSUS ROOF DISPLACEMENT FOR THE DESTRUCTIVE TESTS OF THE ORIGINAL AND EPOXY-REPAIRED STRUCTURES

that this point may represent the transition from uncracked to cracked section properties. This hypothesis was tested against published data on damage to beam-column connections.

Kustu et al.[25] have statistically analyzed the results of laboratory tests on reinforced concrete specimens to determine mean values and standard deviations for joint rotations corresponding to cracking and yielding in beams and columns. They also developed a simple procedure for relating the joint rotations to the interstory drifts. Using their relationship to calculate joint rotations and comparing those rotations with their statistical data, it was calculated that there was a 75% probability of beam cracking corresponding to a roof displacement of 1.0 in. and only a 10% probability of column cracking. The beam rotation corresponding to a roof displacement of 1.0 in. was 40% of the standard deviation above the mean value for beam cracking. Thus, there is a very good statistical basis for identifying the break point in the plot of the base shear as corresponding to the inception of beam cracking in the structure.

A second break in the curve for the base shear in the original structure occurs at about 2.5 in. of roof displacement. Using the relationship and data from Kustu et al., there was a 57% probability of beam yielding corresponding to this point but only a 0.1% probability of column yielding. The beam rotation was less than 2% of the standard deviation above the mean value for beam yielding. Thus, this is a reasonably good statistical basis for identifying the second break point in the base shear curve for the original structure as the inception of beam yielding.

There is no obvious second break point in the base shear curve for the epoxy-repaired structure that might identify yielding in the beams. There does appear to be a slight change in slope at around 3.0 in. of roof displacement, but the curve above that point was based on only a few data points.

Spectral Velocity

The intensity of the motions experienced by the 4-story test structure during the 1979 destructive test can be approximately compared with earthquake excitations by means of spectral response velocities. The displacement response of a multistory building for a given earthquake response spectrum can be determined by using the following equation:[26]

$$d_{ij_{max}} = \frac{\gamma_j \phi_{ij} S_{vj}}{\omega_j} \qquad (5.4)$$

where:

$d_{ij_{max}}$ = maximum displacement of story i in mode j
γ_j = modal participation factor for mode j
ϕ_{ij} = modal deformation of story i in mode j relative to the top-story deformation
S_{vj} = spectral response velocity at the period of mode j
ω_j = circular natural frequency of mode j

Since the maximum velocity of story i in mode j, $v_{ij_{max}}$, is equal to $\omega_j d_{ij_{max}}$, Equation (5.4) can be reversed to calculate the spectral velocity from known floor velocity. Using the amplitude of the roof velocity recorded at Samples 1, 16, and 33 during the destructive test, and assuming that the entire motion was in the first mode, the values for the equivalent spectral velocity are 1.1 in./sec, 15.2 in./sec, and 27.7 in./sec, respectively. In Figure 28, these values are compared with the 5%-damped response spectrum for the north-south component of the 1940 El Centro earthquake.

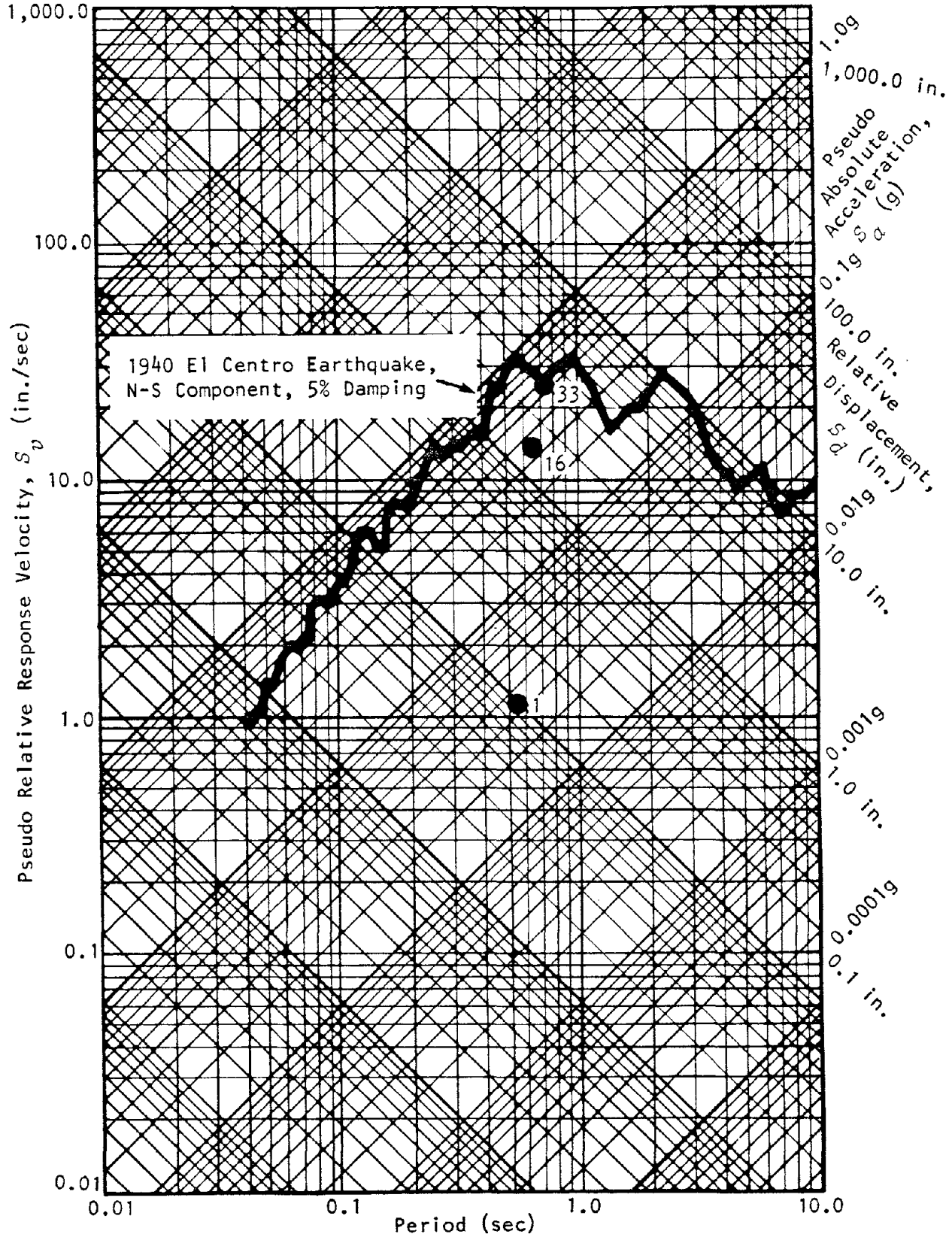

FIGURE 28 EQUIVALENT SPECTRAL VELOCITIES OF SELECTED SAMPLES FROM THE 1979 DESTRUCTIVE DWELL TEST

6. MATHEMATICAL MODELING

Building codes are not specific about stiffness assumptions to be used in modeling the behavior of reinforced concrete structures under lateral forces. This issue was aptly discussed by Freeman et al.,[27] who applied various assumptions to mathematical models for several different structures, including the original 4-story test structure, and compared the calculated stiffnesses of the models with measured stiffnesses of the building.

In this study, additional models of the test structure were developed and compared with the results of the 1974 and 1979 tests. The primary objective was to determine the suitability of several likely models in representing the actual stiffness of the test structure. No attempt was made to determine the suitability of the modeling assumptions in predicting forces internal to the structure.

Mathematical Models for the Test Structure

Four mathematical models were developed to represent the dynamic properties of the test structure in the longitudinal direction. The models differed in member moments of inertia and joint rigidity; however, other aspects of the models were the same. The bases of the columns were fixed against rotation, and frame geometry was determined by centerline-to-centerline dimensions of the beams and columns. Linear elastic behavior was assumed, although it is well known that concrete behaves in a nonlinear fashion, the modulus of elasticity decreasing with increasing strain. The modulus of elasticity was taken to be 3,800,000 psi, which was based on a compressive strength of 4,500 psi.

The moments of inertia for members in Model 1 were based on gross areas of the cross sections. The longitudinal beams were 15 in. deep by 16 in. wide, providing a moment of inertia, I_{gb}, equal to 4,500 in.^{4}. Columns were 14 in. deep by 16 in. wide with a moment of inertia, I_{gc}, of 3,659 in.^{4}. The shapes and periods for the first four modes of this model were determined using the SAP IV program and are presented in Figure 29.

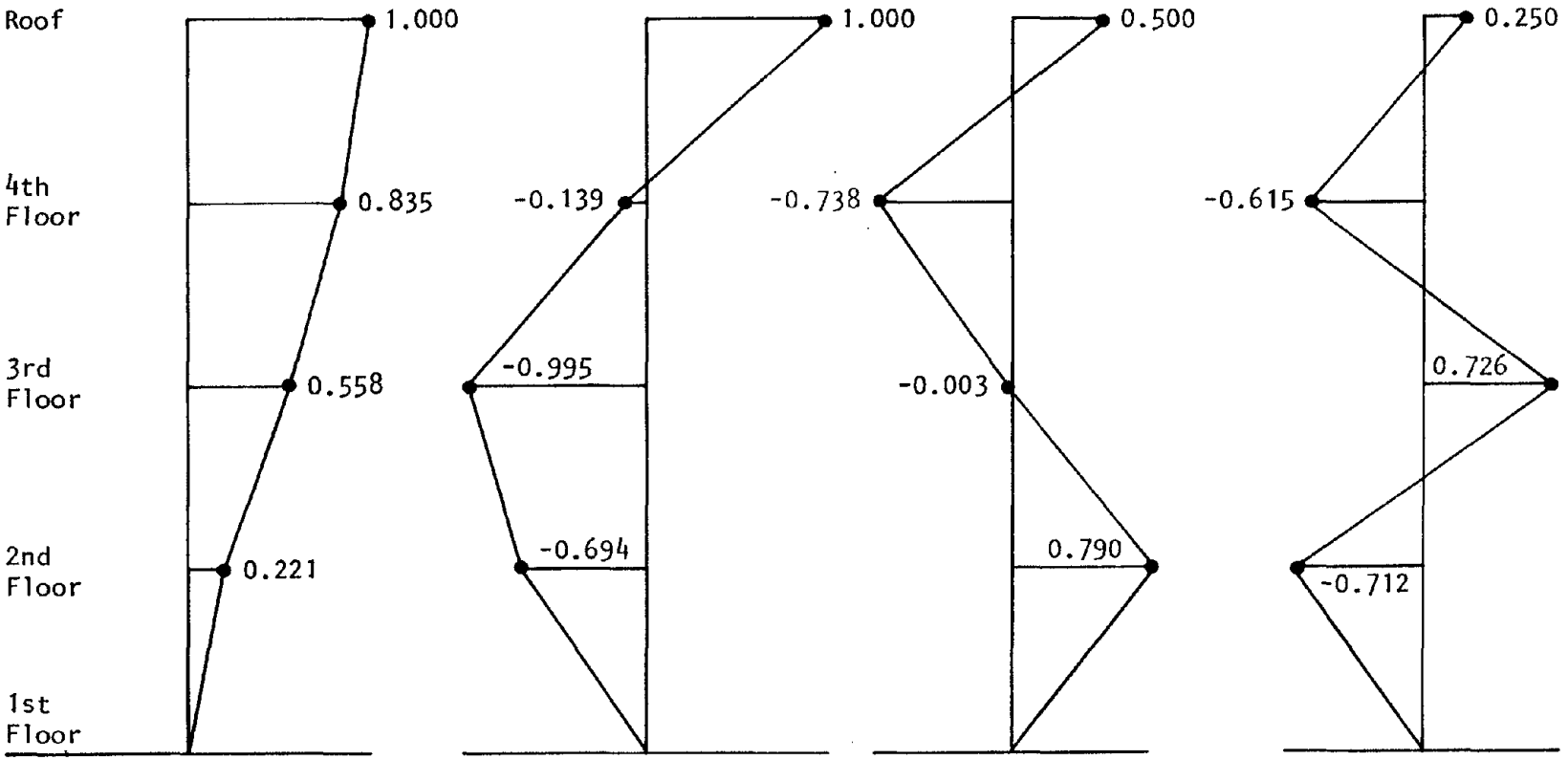

T_1 = 0.443 sec

a. First Mode

T_2 = 0.137 sec

b. Second Mode

T_3 = 0.0712 sec

c. Third Mode

T_4 = 0.0498 sec

d. Fourth Mode

FIGURE 29 MODE SHAPES AND PERIODS DEVELOPED USING THE SAP IV PROGRAM, MOMENTS OF INERTIA BASED ON GROSS AREA

In Model 2, portions of the floor slabs were included in the calculations for beam moments of inertia, according to the provisions of Section 8.10.3 of the ACI 318-77 Code.[6] It should be noted that these guidelines were really intended for gravity load calculations and are not necessarily applicable to lateral force calculations. The beam moments of inertia in this model were 6,480 in.^{4}, or $1.44I_{gb}$. Column moments of inertia remained the same as in Model 1. Mode shapes and periods were determined using the SAP IV program and are presented in Figure 30.

Model 3 uses guidelines provided in the ACI 318-77 Commentary[28] regarding the stiffness of frames that are free to sway. Section 10.10.1 of the commentary suggests that beam moments of inertia be computed as one-half the value based on gross area and that column moments of inertia be computed from the following expression:

$$I = I_g\left(0.2 + \frac{1.2\rho_t E_s}{E_c}\right) \qquad (6.1)$$

where:

I = moment of inertia to be used in analysis

I_g = moment of inertia based on gross area of section

ρ_t = ratio of total longitudinal reinforcement to gross area of section

E_s = modulus of elasticity of reinforcement

E_c = modulus of elasticity of concrete

The columns in all stories were reinforced with six No. 9 bars. The moduli of elasticity were 29,000,000 psi for steel and 3,800,000 psi for concrete. Using Equation (6.1), the column moments of inertia were $0.45I_{gc}$. The results of the SAP IV analysis of Model 3 are presented in Figure 31.

The lengths of the members in all three of these models were based on centerline-to-centerline dimensions; thus, the effects of joint size and rigidity on the stiffness of the models were ignored. The TABS 80 program[29] accounts for joint rigidity by replacing a portion of each end of the members with a rigid link. The length of a rigid link at the end of a

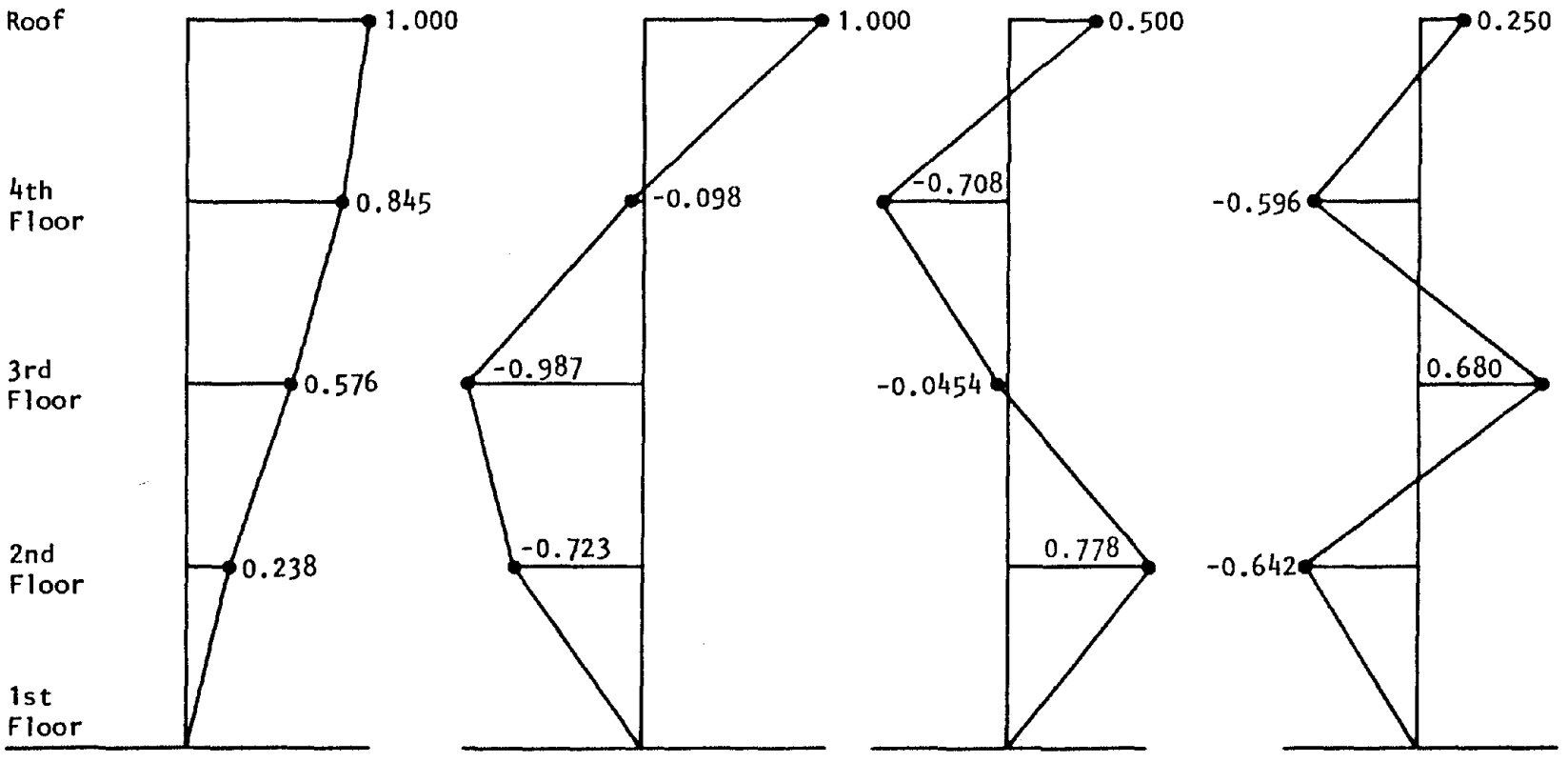

FIGURE 30 MODE SHAPES AND PERIODS DEVELOPED USING THE SAP IV PROGRAM, WITH MOMENTS OF INERTIA BASED ON GROSS AREA AND A PORTION OF THE FLOOR SLAB INCLUDED IN THE BEAMS

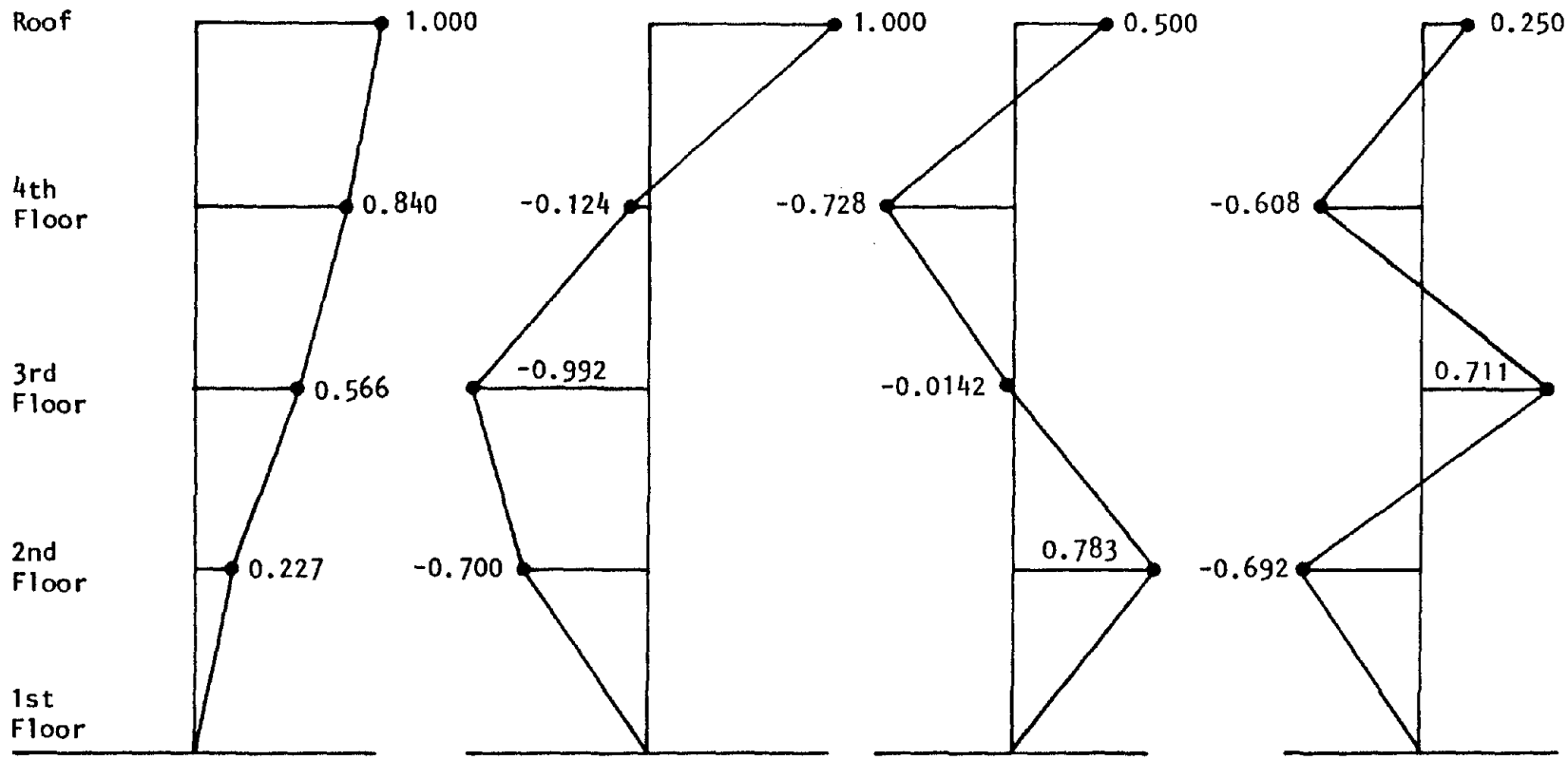

FIGURE 31 MODE SHAPES AND PERIODS DEVELOPED USING THE SAP IV PROGRAM, MOMENTS OF INERTIA BASED ON SECTION 10.10.1 OF THE ACI 318-77 COMMENTARY

beam is the distance from the intersection of the beam and column centerlines to the column face, less one-fourth the beam depth. A rigid link at the end of a column is computed in the converse manner. Prior TABS programs did not reduce the lengths of the links by one-fourth the member depths, a procedure which tended to overestimate joint rigidity. In order to estimate the effect of joint rigidity on the models, the parameters used for Model 1 were used in TABS 80 to create Model 4. The results are illustrated in Figure 32.

Comparison of Models and the Test Structure

The corresponding mode shapes of the four models are all very similar to each other. A visual comparison of the model mode shapes and the measured mode shapes (Figures 18 and 19) demonstrates an excellent agreement in the first and second modes and a fair agreement in the third mode.

Fundamental periods of the models vary considerably from one to another and in comparison with measured values. The fundamental periods are listed in Table 11 along with the different assumptions for the models. The relative stiffnesses for Models 2 and 4 (6.28 and 6.82, respectively) exceed measured values; therefore, these models do not appear to provide realistic representations of the stiffness of the test structure.

For comparison, the relative stiffnesses for Models 1 and 3 are shown in Figure 25. Model 1 appears to provide a fairly good representation of the stiffness of the test structure at low-amplitude motion; Model 3 appears to be more applicable for high-amplitude motion.

When the epoxy-repaired structure had the same stiffness as Model 3, it experienced roof displacements of about 3.5 cm (1.4 in.), zero to peak, with a maximum interstory drift of about 0.5% of the story height. In the discussion on base shear, it was pointed out that there was a high probability that cracking had occurred by the time the roof displacements had reached 2.5 cm (1.0 in.). This confirms that the guidelines of Section 10.10.1 in the ACI 318-77 Commentary (which were the bases for Model 3) are an excellent representation of the cracked-section stiffness of the test structure when deflections were in the order of the code limits.

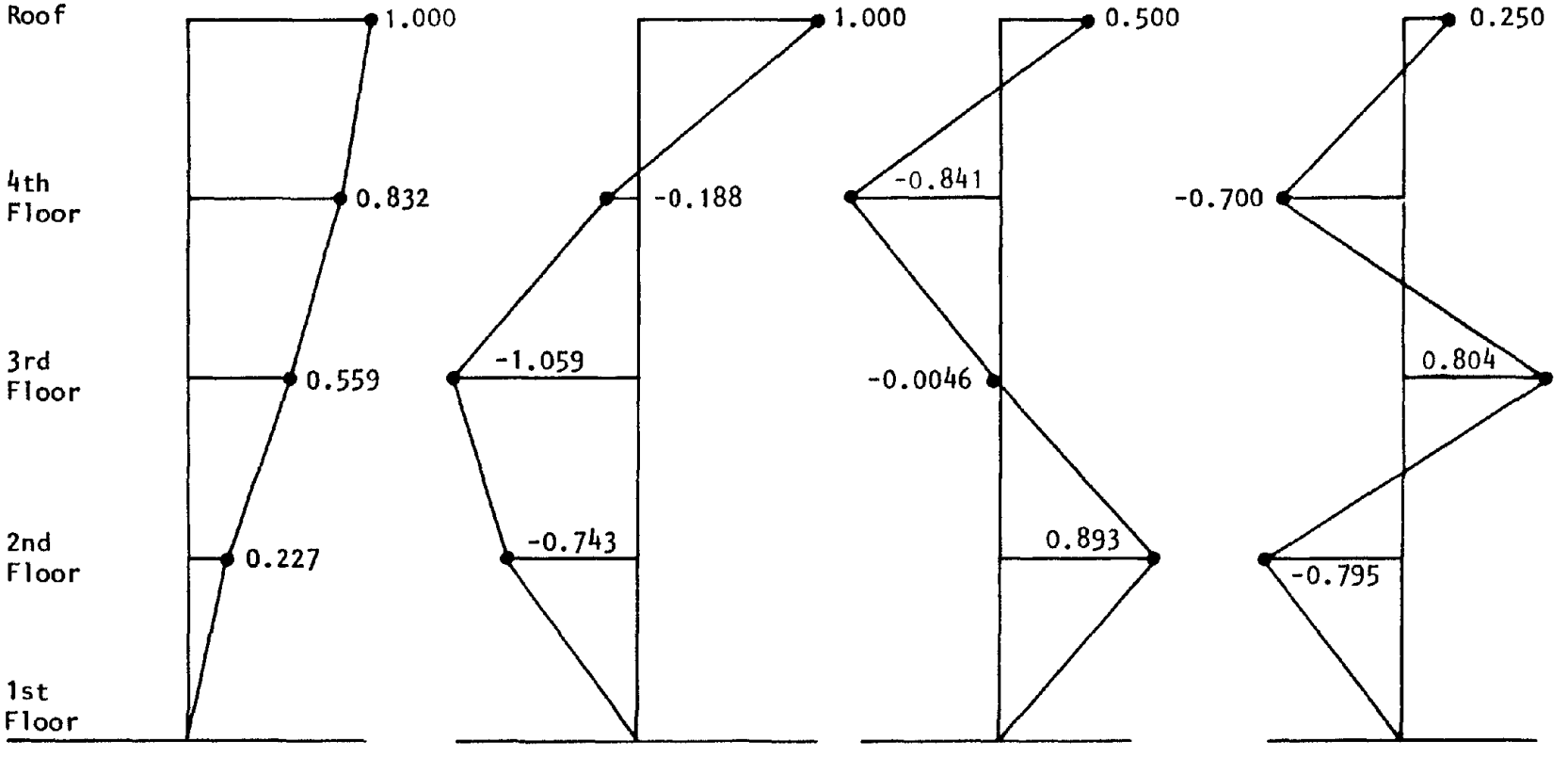

T_1 = 0.383 sec

a. First Mode

T_2 = 0.117 sec

b. Second Mode

T_3 = 0.0588 sec

c. Third Mode

T_4 = 0.0400 sec

d. Fourth Mode

FIGURE 32 MODE SHAPES AND PERIODS DEVELOPED USING THE TABS 80 PROGRAM, WITH RIGID LINKS REDUCED BY 25% OF THE MEMBER DEPTHS

TABLE 11

FUNDAMENTAL PERIOD AND RELATIVE STIFFNESSES

OF MATHEMATICAL MODELS

Model	Assumptions*	I/I_g †		Period, T (sec)	Relative Stiffness, f^2 (Hz^2)
		Beams	Columns		
1	Moments of inertia based on gross area	1.0	1.0	0.443	5.10
2	Moments of inertia of beams include portion of slabs	1.44	1.0	0.399	6.28
3	Moments of inertia based on ACI 318-77	0.5	0.445	0.634	2.49
4	Moments of inertia based on gross area and rigid links for physical joints	1.0	1.0	0.383	6.82

*Assumptions common to all models listed in text

†I = moment of inertia of model
I_g = moment of inertia for gross area

Theoretical Capacities

Theoretical model capacities provide another means for comparing the behavior of mathematical models with that of the actual structure. Moment capacities for the longitudinal beams at the second through fourth floors and the roof were computed for both working stress and ultimate strength. The largest bending moments created by dead and lateral loads combined are created at the ends of the beams with compression on the bottom of the beams. Therefore, only capacities at those locations were of interest and are presented in Table 12. The assumed properties of the concrete were unconfined compressive strength of 4,500 psi, allowable working stress of 2,000 psi, and modulus of elasticity of 3,800,000 psi. The properties of the reinforcing were yield stress of 50,000 psi, allowable working stress of 20,000 psi, and modulus of elasticity of 29,000,000 psi. The beam reinforcement schedule was obtained from Reference 11.

Three dead-load conditions were analyzed: (1) the weight of the bare frame, (2) the frame weight plus 19,000 lb distributed over the third floor to represent the weight of the vibration generator in the 1974 tests, and (3) the frame weight plus 28,500 lb on the third floor to represent the 1979 vibration generator. The lateral load consisted of forces at each floor level, with each force proportional to the first-mode shape (obtained from Test M-1-L-PE) times the weight of the floor. The analyses were conducted using Model 3 because it gave the best representation of cracked-section stiffness.

By adding scaled values of the beam bending moments obtained from the lateral force analysis to the dead-load moments, it was possible to determine the amount of lateral load needed to reach the working-stress and ultimate-strength capacities. For comparative purposes, the arrivals at these capacities are identified by the roof displacement corresponding to the appropriately scaled lateral load. These values of roof displacements are listed in Table 13.

The roof displacements corresponding to first arrivals at working-stress capacity and ultimate-strength capacity for the bare frame have been marked on Figure 25. This provides a qualitative comparison of the performance of

TABLE 12

BEAM MOMENT CAPACITIES

Floor	Working Stress Moment Capacity (kip-ft)	Ultimate Strength Moment Capacity (kip-ft)
Roof	40	91
Fourth	47	107
Third	59	124
Second	59	132

TABLE 13

LATERAL ROOF DISPLACEMENT CORRESPONDING TO CAPACITY THRESHOLDS FOR VARIOUS DEAD-LOAD CONDITIONS

Dead Load	Roof Displacement (cm)	
	Working Stress	Ultimate Strength
Bare frame	0.87	3.12
Bare frame with 1974 vibration generator	0.17	2.40
Bare frame with 1979 vibration generator	0.0*	2.02

*The dead-load moments in the third floor exceed the working-stress moment capacity by about 10%.

the test structure in relationship to probable design capacities. The first arrival at ultimate-strength capacity is designated as the yield capacity because the development of a plastic hinge within a rigid frame is the theoretical yield capacity of the frame.

The roof displacements corresponding to the first arrivals at ultimate-strength capacity for the bare frame, the bare frame plus the 1974 vibration generator, and the bare frame plus the 1979 vibration generator are shown in Figure 27. The previous analysis of this plot of base shear versus roof displacement suggested that the break in the curve at a roof displacement of about 1.0 in. indicated a transition from uncracked to cracked sections. However, the yield capacity calculations suggest that the break would indicate the establishment of the first plastic hinge. The calculations for yield capacity probably underestimate the real yield of the test structure.

7. SUMMARY AND CONCLUSIONS

The results of this study have shown that, for low-amplitude motion, the epoxy-repaired structure was slightly less stiff than the original undamaged structure. This was expected because not all cracks could be repaired and also because the epoxy compound that was used was a more flexible material than concrete. However, the destructive-test data show that, as the amplitude of the structure's response increased, the difference in stiffness between the epoxy-repaired structure and the original structure decreased. At large deflections associated with severe damage, the stiffness of the epoxy-repaired structure did not degrade as much as the stiffness of the original structure.

The epoxy-repaired structure was less severely damaged than the original structure, with cracking more widely dispersed and less concentrated at the joints. This suggests that the epoxy-injection procedure may have created better joints in the repaired structure than previously existed in the original structure. One would suspect that the epoxy improved the bonding between the reinforcing bars and the concrete in the joint. This supposition seems to contradict the results from the severe cyclic tests reported elsewhere.[3] However, it should be noted that those tests were conducted on the equivalent of interior joints and resulted in severe bond degradation. In contrast, the joints in the 4-story test structure are all exterior ones.

On the basis of these test results, the epoxy-injection technique appears to be a satisfactory method for repairing earthquake-damaged structures. However, it is important to note that, when subjected to high temperatures, such as in a building fire, the epoxy compounds will suffer loss of strength and may even burn. Furthermore, there is no current information on the effect of long-term aging on epoxy compounds.

A mathematical model using cracked section properties based on the guidelines in Section 10.10.1 of the ACI 318-77 Commentary appeared to be a good

model for representing the stiffness of the 4-story structure at its approximate yield capacity. When the stiffness of the epoxy-repaired structure corresponded to that of the model, the drift was approximately equal to the *UBC* drift limits of 0.5% of the story height. However, when the original structure was at that same stiffness, the drift was about 50% larger than the *UBC* drift limits.

REFERENCES

1. Mahin, S. A., and V. V. Bertero, *Rate of Loading Effects on Uncracked and Repaired Concrete Members*, EERC Report 72-9, Earthquake Engineering Research Center, University of California, Berkeley, 1972.

2. Celebi, M., and J. Penzien, *Hysteretic Behavior of Epoxy-Repaired Reinforced Concrete Beams*, EERC Report 73-5, Earthquake Engineering Research Center, University of California, Berkeley, 1973.

3. Popov, E. P., and V. V. Bertero, "Repaired R/C Members Under Cyclic Loading," *Proceedings*, 5th Congress of the Yugoslav Association of Structural Engineers, Budva, Montenegro, Yugoslavia, September 30 through October 5, 1974.

4. Hidalgo, P., and R. W. Clough, *Earthquake Simulator Study of a Reinforced Concrete Frame*, EERC Report 74-13, Earthquake Engineering Research Center, University of California, Berkeley, December 1974.

5. Clough, R. W., and J. Gidwani, *Reinforced Concrete Frame 2: Seismic Testing and Analytical Correlation*, EERC Report 76-15, Earthquake Engineering Research Center, University of California, Berkeley, June 1976.

6. ACI Committee 318, *Building Code Requirements for Reinforced Concrete*, American Concrete Institute, Detroit, Michigan, 1977.

7. International Conference of Building Officials, *Uniform Building Code*, Whittier, California, 1961.

8. Blume, J. A., "A Reserve Energy Technique for the Design and Rating of Structures in the Inelastic Range," *Proceedings*, Second World Conference on Earthquake Engineering, Tokyo, July 1960.

9. Blume, J. A., N. M. Newmark, and L. H. Corning, *Design of Multistory Reinforced Concrete Buildings for Earthquake Motions*, Portland Cement Association, Skokie, Illinois, 1961.

10. International Conference of Building Officials, *Uniform Building Code*, Whittier, California, 1982.

11. John A. Blume & Associates Research Division, *Concrete Test Structures: First Progress Report on Structural Response*, JAB-99-29, San Francisco, 1968.

12. Freeman, S. A., *Concrete Test Structures: Second Progress Report on Structural Response*, JAB-99-50, John A. Blume & Associates Research Division, San Francisco, 1971.

13. Raggett, J. D., *Influence of Nonstructural Partitions on the Dynamic Response Characteristics of Structures*, JAB-99-94, John A. Blume & Associates Research Division, San Francisco, July 1972.

14. Kost, E. G., *Nonlinear Dynamic Analysis of Frames with Filler Panels*, JAB-99-100, John A. Blume & Associates Research Division, San Francisco, November 1972.

15. Kost, E. G., W. Weaver, Jr., and R. B. Barber, "Nonlinear Dynamic Analysis of Frames with Filler Panels," *Journal of the Structural Division*, ASCE, Vol. 100, No. ST4, 1974.

16. Freeman, S. A., C. K. Chen, and R. M. Czarnecki, "Dynamic Response Characteristics of Reinforced Concrete Structures," *Proceedings*, ASCE/EMD Specialty Conference on Dynamic Response of Structures, University of California, Los Angeles, March 1976.

17. Chen, C. K., R. M. Czarnecki, and R. E. Scholl, *Vibration Tests of a 4-Story Reinforced Concrete Test Structure*, JAB-99-119, URS/John A. Blume & Associates, Engineers, San Francisco, January 1976.

18. _____, "Vibration Tests of a 4-Story Concrete Structure," *Proceedings*, Sixth World Conference on Earthquake Engineering, New Delhi, January 1977.

19. _____, "Destructive Vibration Test of a 4-Story Concrete Structure," *Proceedings*, The Douglas McHenry International Symposium on Concrete and Concrete Structures, Mexico City, October 1976.

20. Adhesive Engineering Co., *Concresive 1050-15*, Technical Bulletin AE 202/7, San Carlos, California, November 1968.

21. Smallwood, D. O., and N. F. Hunter, "A Transportable 56-kN, 200-mm Displacement Hydraulic Shaker for Seismic Simulation," *Proceedings*, Institute of Environmental Science, 1975.

22. Navarro, R., and G. M. Wuollet, *The L-7 Velocity Seismograph Shaking-Table Results*, NOAA Technical Report, ERL 254-ESL, U.S. Department of Commerce, National Oceanic and Atmospheric Administration, Environmental Research Laboratories, 1972.

23. Nigam, N. C., and P. C. Jennings, "Calculation of Response Spectra from Strong-Motion Earthquake Records," *Bulletin of the Seismological Society of America*, Vol. 59, No. 2, pp. 909-922, April 1969.

24. Bathe, K.-J., E. L. Wilson, and F. E. Peterson, *SAP IV, A Structural Analysis Program for Static and Dynamic Response of Linear Systems*, EERC Report 73-11, Earthquake Engineering Research Center, University of California, Berkeley, 1974.

25. Kustu, O., D. D. Miller, and S. T. Brokken, *Development of Damage Functions for High-Rise Building Components*, JAB-10145-2, URS/John A. Blume & Associates, Engineers, San Francisco, California, October 1982.

26. URS/John A. Blume & Associates, Engineers, *Effects Prediction Guidelines for Structures Subjected to Ground Motion*, JAB-99-115, San Francisco, California, July 1975.

27. Freeman, S. A., R. M. Czarnecki, and K. K. Honda, "Significance of Stiffness Assumptions on Lateral Force Criteria," *Reinforced Concrete Structures Subjected to Wind and Earthquake Forces*, Publication SP-63, American Concrete Institute, Detroit, Michigan 1980.

28. ACI Committee 318, *Commentary on Building Code Requirements for Reinforced Concrete*, American Concrete Institute, Detroit, Michigan, 1977.

29. Wilson, E. L., H. H. Dovey, and A. Habibullah, *Three-Dimensional Analysis of Building Systems, TABS*, Computers/Structures International, Berkeley, California, June 1980.